Assessing the seismic coupling of shallow continental faults and its impact on seismic hazard estimates: a case-study from Italy.

Michele M. C. Carafa [(1)], Gianluca Valensise [(2)], Peter Bird [(3)]

[1] Istituto Nazionale di Geofisica e Vulcanologia – INGV, Sezione di Sismologia e Tettonofisica, L'Aquila, Italy. Email: *michele.carafa@ingv.it* ORCID ID: 0000-0001-5463-463X

[2] Istituto Nazionale di Geofisica e Vulcanologia – INGV, Sezione di Sismologia e Tettonofisica, Roma, Italy. Email: *gianluca.valensise@ingv.it* ORCID ID: 0000-0001-7631-1903

[3] Department of Earth, Planetary and Space Sciences, University of California, Los Angeles, USA. Email: *pbird@epss.ucla.edu* ORCID ID: 0000-0001-9034-1287

Accepted date. Received date; in original form date

Abbreviated title for page headings: *Seismic coupling of active faults in Italy*

Corresponding author: Michele M. C. Carafa, michele.carafa@ingv.it

Summary

We propose an objective and reproducible algorithmic path to forecast seismicity in Italy from long-term deformation models. These models are appropriate for Italy and its neighboring countries and seas thanks to the availability of rich, reliable and regularly updated historical earthquake and seismogenic fault databases, and to the density of permanent GPS stations. However, so far little has been done to assess the seismic coupling of Italian active faults, i.e. to quantify their ability to release earthquakes. This must be determined in order to use geodetic and active faulting observations in alternative seismicity models, to overcome possible limitations of the earthquake record for the assessment of seismic hazard. We use a probabilistic method to assign upper crustal earthquakes from the historical catalogue to their presumed causative faults, then collect all the events into three subcatalogues corresponding to the compressional, extensional and strike-slip faulting classes. We then determine the parameters of their Gutenberg-Richter frequency/magnitude relations using maximum-likelihood methods and integrate these distributions to estimate the long-term seismic moment rate for each class. Finally, we compare these seismicity rates to the long-term tectonic deformation based on GPS data, thus determining the coupled thickness (and estimating seismic coupling) for each fault class. We find that in our study region the seismic coupling and the related coupled thickness is on average two times larger for extensional than for compressional faults. As for the spatial distribution of earthquake rates, a larger number of events is predicted for the extensional settings of the Apennines chain, in agreement with the inferred seismic coupling but also with the long-term strain rates. We also find that the frequency/magnitude distributions indicate that the largest earthquakes occur in extensional settings, whereas compressional faults are expected to host comparatively smaller events.

Keywords: Continental tectonics: compressional; Continental tectonics: extensional; Earthquake interaction, forecasting and prediction; Earthquake hazard; Seismicity and tectonics

1. Introduction

Over the past few years a growing number of seismicity and seismic hazard models have relied on information from tectonics and active faulting to obtain alternative estimates of the expected ground shaking (e.g., Stirling et al., 2012; Field et al. 2014; Woessner et al. 2015; Kastelic et al. 2016), supplementing those derived from traditional extrapolation of the seismic catalog. At least in the most earthquake-prone areas of the world, including Italy, fault-based seismic hazard is slowly but steadily replacing – or at least complementing - the seismicity-based or zone-based approaches used in the past (e.g. Stucchi et al. 2011). The core of these largely empirical-statistical applications is the projection into the future of historical seismicity as generated by "seismic zones", finite areas each point of which is presumed to have the same probability of releasing earthquakes following a specific magnitude-frequency distribution. The main drawback of such applications rests in the often short and spatially-incomplete record of earthquake occurrence, which fails to adequately sample the long-term average of seismic release. A comparison of the characteristic length of the earthquake record conducted for Italy (Stucchi et al. 2004), a country that features an especially long seismic history, with the expected long-term slip rate for local faults (Valensise & Pantosti 2001a; Basili et al. 2008) suggests that the activity of two out of three sources of potentially damaging events (Mw 5.5+) may have gone undetected so far. This implies that not even one complete "seismic cycle" could be represented by the available earthquake sample, let alone that a statistically-sound forecast should encompass at least a few complete "seismic cycles."

These limitations can be overcome with innovative approaches which use other datasets including fault locations and slip rates, velocities of benchmarks from Global Positioning System (GPS) geodesy, and azimuths of the most-compressive horizontal principal stress (SHmax) (Stucchi et al.

2011; Bird & Liu 2007; Bird & Kreemer 2015). Over the past two decades various investigators have developed databases and models of potentially active faults, GPS measurements and long-term deformation patterns for the whole Italian territory (Basili et al. 2008; Barba et al. 2010; Devoti et al. 2014; Montone & Mariucci 2016). Each of these datasets, however, is affected by significant limitations that are quite hard to overcome: for instance, the tectonic motions documented by GPS data are inevitably mixed with short-term transients (Carafa & Bird 2016); reliable magnitude estimates and focal mechanisms are available for only a subset of past earthquakes; and, as pointed out earlier, the earthquake record is too short (Stucchi et al. 2004).

The dataset on active faults in Italy is affected by several major limitations: a) fault mapping remains incomplete, especially in offshore areas, though the progressive availability of data from the oil industry is helping to fill the main gaps; b) precise slip-rates are few; and c) very little is known about the seismic coupling of Italian faults. The concept of seismic coupling was originally introduced by Kanamori (1971) following an investigation of great earthquakes of the circum-Pacific belt. Seismic coupling, which is dimensionless and no more than unity, is the fraction of fault slip in the frictional regime that occurs in earthquakes. The issue was pursued by scientists working on well-known plate-boundaries zones (e.g. Cowie et al. 1993; McCaffrey 1997; Bird & Kagan 2004; Becker & Meier 2010); but so far it has received limited attention in areas of spread deformation where seismic hazard is distributed on complex systems of active faults, such as in the western US and in Europe. As a result, it is common practice to assume that the coupling simply equals one, implying that all tectonic deformation above the brittle/ductile transition depth translates into earthquakes release (e.g., Woessner et al. 2015 in the context of the calculation of the 2013 Seismic Hazard Map of Europe). There is growing evidence, however, that this may not be a general rule, particularly in tectonic areas undergoing compression such as the Hellenic Arc (Bird & Kagan 2004; Bird et al. 2009; Howe & Bird 2010). It follows that assessing the seismic coupling in all tectonic environments that contribute to a country's seismic hazard is a fundamental prerequisite for a correct use and integration of the active faulting, GPS and seismicity databases and hence for achieving more reliable estimates than those obtained by means of statistical methods.

Our goal is to assess the seismic coupling of Italian faults, with the aim of (a) understanding the fundamentals of this property of active faults and – even more importantly – (b) avoiding an unjustified overestimate of seismic hazard in areas where the coupling is very low. To this end we retrace all steps of the seminal work of Bird & Kagan (2004) at the scale of the central Mediterranean, with the aim to propose an objective formulation for calculating the seismic coupling and corner magnitudes and forecasting the seismicity for Italy.

We use the fault kinematics reported in the current version of the Database of the Individual Seismogenic Sources (DISS) (v. 3.2.0: Basili et al. 2008; DISS Working Group 2015) to classify each fault as belonging to one of three classes: compressional, extensional, or strike-slip. We use a Bayesian method to assign each shallow earthquake from the historical catalogue CPTI15 (Catalogo Parametrico dei Terremoti Italiani 2015: Rovida et al. 2016) to its presumed causative fault. Finally, we collect the earthquakes into three subcatalogues corresponding to the three fault classes. We then analyze the earthquake counts and magnitudes in these subcatalogues to determine the parameters of their Gutenberg-Richter frequency/moment relations using maximum-likelihood methods (Kagan, 2002). Next we integrate these distributions to estimate the long-term seismic moment rate for each class. We refer to the long-term kinematic deformation models recently published by Carafa & Bird (2016) and propose a new formulation to determine the long-term tectonic moment rate of the crust. We then compare the obtained seismic moment rates to tectonic moment rates to forecast seismicity

for Italy and to determine for each class the coupled lithosphere thickness as defined by Bird & Kagan (2004).

2. Methodology

The natural way to connect recent tectonic activity to seismicity is to predict long-term-average seismic moment rates $\dot{M}_{seis}$ for deforming volumes of the lithosphere using the long-term tectonic moment rate $\dot{M}_{tect}$. Over a sufficiently long time, the mean rate of elastic strain in the lithosphere should approach zero and $\dot{M}_{tect}$ should be expressed either as earthquakes or as aseismic frictional sliding. Then, we can relate these two long-term estimates by

$$\dot{M}_{seis} = c \cdot \dot{M}_{tect} \qquad (1)$$

where c is referred to as "seismic coupling". In order to include simultaneously the contribution of very large but very rare earthquakes and of small but very frequent events and to avoid any volatile and subjective estimate of c, we use frequency-magnitude distributions to calculate $\dot{M}_{seis}$.

Among different models of the frequency-magnitude distributions, the Tapered Gutenberg-Richter (TGR) has several advantages: it fits the long-term seismicity better than other distributions, it is computationally simple and manageable, it is easy to simulate and its parameters are less correlated than the ones of other distributions (Kagan 2002). Furthermore, the maximum-likelihood determination of its distribution parameters has smaller standard errors than those affecting other distributions. Conversely, distributions with hard maximum-magnitude cut-offs (the characteristic distribution or the truncated Pareto distribution) yield seismic moment rates that are significantly higher than the TGR (Kagan 2002).

The TGR describes the fraction G of earthquakes with moment exceeding M as

$$G(M, M_t, \beta, M_c) = \left(\frac{M}{M_t}\right)^{-\beta} \exp\left(\frac{M_t - M}{M_c}\right) \qquad (2)$$

where M_t is the threshold moment for completeness of the catalog, β is the asymptotic spectral slope at small moments, and M_c is the corner moment. Thus, the seismic moment rate $\dot{M}_{seis}$ can be calculated with the total number of earthquakes α_0 with $M \geq M_t$ (Kagan 2002):

$$\dot{M}_{seis} = \frac{\alpha_0 \cdot M_t^{\beta} \cdot \Gamma[2-\beta]}{1-\beta} \cdot M_c^{1-\beta} \cdot \exp[M_t / M_c] \qquad (3)$$

where Γ is the gamma function. .

Our method of estimating $\dot{M}_{tect}$ in Equation (1) assumes that we have access to fields of long-term (permanent, non-elastic) strain rates in the horizontal plane at the Earth surface. Diagonalization of the 2×2 horizontal-plane strain-rate tensors gives the principal horizontal values $\dot{\varepsilon}_{1h}$ (more negative or compressional) and $\dot{\varepsilon}_{2h}$ (more positive or extensional) and their associated principal axis directions. Then, we can infer the vertical (principal) strain-rate from incompressibility of permanent strain $\dot{\varepsilon}_{rr} = -(\dot{\varepsilon}_{1h} + \dot{\varepsilon}_{2h})$. The three orthogonal principal axes and the three principal values of the long-

term strain-rate tensors are now fully defined and can be re-labelled as $\hat{\dot{\varepsilon}}_1 \perp \hat{\dot{\varepsilon}}_2 \perp \hat{\dot{\varepsilon}}_2$ and $\dot{\varepsilon}_1 \le \dot{\varepsilon}_2 \le \dot{\varepsilon}_3$, respectively. In the real world, the more active conjugate fault set has its slip-rate vectors in the plane containing the principal axes $\hat{\dot{\varepsilon}}_1$ and $\hat{\dot{\varepsilon}}_3$. In addition, a less active conjugate fault set is likely to exist (except in special cases) with slip-rate vectors in the plane containing both $\hat{\dot{\varepsilon}}_2$ and the principal axis whose strain-rate has opposite sign, so $\hat{\dot{\varepsilon}}_3$ if $\dot{\varepsilon}_2 < 0$ or $\hat{\dot{\varepsilon}}_1$ if $\dot{\varepsilon}_2 \ge 0$. An alternative way to state these relations is to define:

$$\dot{\varepsilon}_{\text{great}} = \sup(|\dot{\varepsilon}_1|, |\dot{\varepsilon}_2|, |\dot{\varepsilon}_3|) \quad (4)$$

$$\dot{\varepsilon}_{\text{least}} = \inf(|\dot{\varepsilon}_1|, |\dot{\varepsilon}_2|, |\dot{\varepsilon}_3|) \quad (5)$$

$$\dot{\varepsilon}_{\text{mid}} = \dot{\varepsilon}_{\text{great}} - \dot{\varepsilon}_{\text{least}} \quad (6)$$

The formulation by Kostrov (1974) links deformation to moment rate release and assumes that the mean deformation rate ε_{ij} in the volume $\Delta V = A \cdot z$ is due to N earthquakes that occurred during the time Δt , with

$$\dot{\varepsilon}_{ij} = \frac{1}{2\mu \Delta V \Delta t} \sum_{1}^{N} (M_0)_{ij} \quad (7)$$

where μ is the elastic shear modulus. Subsequently Ward (1994) translated strain-rates into rates of potential moment release relying on the formulation of Kostrov (1974) and reducing the original tensor $(M_0)_{ij}$ to a scalar M_0 by replacing the tensor strain-rate by the greatest absolute value of any principal strain-rate, $\dot{\varepsilon}_{\text{great}}$, thus obtaining:

$$\dot{M}_{\text{tect}} = k \cdot \mu \cdot A \cdot z \cdot \dot{\varepsilon}_{\text{great}} \quad (8)$$

with $k=2$ and z, the seismicity cutoff (coincident with the brittle/ductile transition), defined as seismogenic thickness. In Appendix 1 we show that a different k factor (not the $k=2$ of *Ward* (1994)) needs to be considered if the active-fault planes in the modeled volume of lithosphere are not at angles of $\theta = 45°$ from $\hat{\dot{\varepsilon}}_{\text{great}}$.

In Appendix 1 we also show that

$$\dot{M}_{\text{tect}} = \mu \cdot A \cdot z \cdot \left(\frac{1}{\sin\theta_1 \cos\theta_1} \cdot \dot{\varepsilon}_{\text{med}} + \frac{1}{\sin\theta_2 \cos\theta_2} \cdot \dot{\varepsilon}_{\text{small}} \right) \quad (9)$$

where θ_1 and θ_2 are the average angles dividing respectively the fault planes from $\dot{\varepsilon}_{\text{great}}$ in the $\left(\hat{\dot{\varepsilon}}_{\text{great}}, \hat{\dot{\varepsilon}}_{\text{med}}\right)$ plane and in the $\left(\hat{\dot{\varepsilon}}_{\text{great}}, \hat{\dot{\varepsilon}}_{\text{least}}\right)$ plane.

Thus, replacing equation (9) in Equation (1), we can write

$$\dot{M}_{\text{seis}} = c \cdot z \cdot \mu \cdot A \cdot \left(\frac{\dot{\varepsilon}_{\text{med}}}{\cos(\theta_1)\sin(\theta_1)} + \frac{\dot{\varepsilon}_{\text{least}}}{\cos(\theta_2)\sin(\theta_2)} \right) \quad (10)$$

where we refer to the product $c \cdot z$ of the right term as the "coupled thickness of seismogenic lithosphere" (Bird *et al.* 2002; Bird & Kagan 2004), while $A \cdot \left(\frac{\dot{\varepsilon}_{\text{med}}}{\cos(\theta_1)\sin(\theta_1)} + \frac{\dot{\varepsilon}_{\text{least}}}{\cos(\theta_2)\sin(\theta_2)} \right)$ is the "diffusivity" of the deforming volume of the lithosphere, because of its SI units of $m^2\ s^{-1}$. Alternatively, it was called "potency rate per unit depth" by Bungum (2007).

Available data on seismicity and active tectonics allow us to estimate $\dot{M}_{\text{seis}}$ and the diffusivity for large parts of the lithosphere, whereas an independent estimation of coupling and coupled thickness is still difficult to obtain. Thus, we rely on seismicity and active tectonics, calculating the coupled thickness (and seismic coupling) for large volumes of the lithosphere as:

$$\langle cz \rangle = \frac{\frac{\alpha_0(k) \cdot M_t^{\beta} \cdot \Gamma[2-\beta]}{1-\beta} \cdot M_c^{1-\beta} \cdot \exp[M_t / M_c]}{\mu \cdot A \cdot \left(\frac{\dot{\varepsilon}_{\text{med}}}{\cos(\theta_1)\sin(\theta_1)} + \frac{\dot{\varepsilon}_{\text{least}}}{\cos(\theta_2)\sin(\theta_2)} \right)} \qquad (11)$$

3. Input datasets and modeling procedures

3.1 Spatial definition of the study area

One of the most enigmatic aspects of Central Mediterranean neotectonics is the seismicity of the Calabrian subduction zone. From the beginning of our work we have been aware that the elusive behavior of this subduction zone affects all our datasets (historical catalogue, active fault database, GPS measurements). The subduction interface is expected to exhibit a frictional/elastic behavior and to generate large earthquakes, whose effects on-land in Calabria and Eastern Sicily would be mitigated by distance and the greater focal depth compared to upper-crustal earthquakes. Thus the magnitudes and locations of subduction-interface earthquakes may have been reported with especially large uncertainties in historical catalogues. We expect such earthquakes to occur at 10-35 km depth along the subduction interface, whose surface projection in southeastern Calabria overlaps with some large back-arc extensional faults capable of *m*7+ earthquakes (Tiberti *et al.* 2016), making a hypothetic assignment of a historical earthquake inherently non-unique. For instance, Guidoboni *et al.* (2000) found archeological evidence for a large earthquake in the Messina Straits in the second half of the IV century A.D., but regarded it simply as a predecessor of the catastrophic 28 December 1908 (*m*=7.1) earthquake rather than as an event generated by a source unknown to them. Furthermore, for GPS stations located in Calabria and Sicily an unknown amount of interseismic strain accumulation from this supposedly-locked subduction zone (whose slip rate is currently undetermined) is expected to perturb the short-term deformation patterns, resulting in an incorrect estimation of the long-term tectonic moment-rate for the subduction, back arc and forearc regions combined. Finally, we are aware that the identification and the investigation of weakly active faults is more difficult offshore than it is onland, which suggests to include in our calculations only well investigated offshore areas.

On these grounds, and to avoid any error in calculating the seismicity parameters for Italy, we decided to exclude all the earthquakes falling outside the dashed red polyline shown in Figure 1. In Calabria the border line of this region roughly coincides with the surface projection of the 35-km isobath of the subduction interface (Tiberti *et al.* 2016). Hence, seismicity is forecast only for the portion of the Italian peninsula encircled by the black polyline, thus leaving out Calabria, Sicily, and almost all offshore areas. The different areal coverage between the black and dashed red polylines is motivated by two contrasting requirements. On the one hand we seek to include the largest possible number of

earthquakes for a robust estimation of seismicity parameters for all three fault classes (compressional, extensional, and strike-slip); to this end the inclusion of Calabria and Sicily would be recommended (and valuable) because geological and seismological evidence suggests that crustal seismogenic processes in this reach of Italy do not differ much from those seen in the rest of the country. But on the other hand, including data from these regions, for which any long-term (tectonic and seismic) estimation of moment rate is inherently ambiguous and highly subjective, could lead to a dramatic bias in $\langle cz \rangle$ estimations.

3.2 Historical catalogue

The CPTI15 catalogue (Rovida et al. 2016) is the latest version of the Italian earthquake catalog, which has steadily evolved both in terms of structure and contents over the past 20 years. For the version used in this work the time window has been expanded to 2013 and the supporting dataset includes a number of new macroseismic data. The catalogue supplies both macroseismic and instrumental magnitude determinations, if available, together with uncertainty estimates. Macroseismic locations and magnitudes of onshore events are computed by means of the latest version of the Boxer code (Gasperini et al. 1999), while for offshore events they are based on the method proposed by Bakun & Wentworth (1997). The catalogue does not provide any information on focal mechanisms.

Several studies have investigated and assessed the completeness of the CPTI catalogue using both historical (Stucchi et al. 2004) and statistical (Albarello, 2001) approaches. Shorlemmer et al. (2010) analyzed a previous version of the same catalogue using the Maximum Curvature method and the Entire Magnitude Range method (Woessner & Wiemer, 2005). Their findings on the completeness threshold magnitude (m_t =4.7, conservatively set to m_t=4.8; completeness starting in the year 1900) agrees rather well with that obtained from the historical (m_t=4.7; completeness starting in the year 1871) and statistical approaches (m_t=4.7; completeness starting in the year 1920). In this work we assume for CPTI15 the year 1880 as the beginning of the completeness window for m_t=4.8. Selecting earthquakes based on these thresholds resulted in 405 events for the greater Italian region (dashed red polyline in Figure 1) and 346 for the smaller Italian region (black polyline in Figure 1) where we will forecast seismicity.

3.3 Fault database

The Database of Individual Seismogenic Sources (DISS) is currently the only comprehensive and consistently updated compilation of seismogenic faults available for the broader Italian peninsula. Over the past two decades the DISS Working Group identified and characterized seismogenic sources capable of producing $m \geq 5.5$ earthquakes (Valensise & Pantosti 2001b; Basili *et al.* 2008, Kastelic *et al.* 2013; Vannoli *et al.* 2015; Tiberti *et al.* 2016). The DISS Working Group relies on published data but also on original fieldwork (e.g. Kastelic *et al.* 2008), geomorphologic analyses (Vannoli *et al.* 2004; Burrato *et al.* 2012), and interpretations of seismological and geophysical data (Maesano *et al.* 2013, 2015).

In this work we use the Composite Seismogenic Sources reported in v. 3.2.0 of the database (*DISS Working Group* 2015). These are regional, unsegmented fault systems each of which includes an unspecified number of active and seismogenic faults capable of m=5.5 and larger earthquakes. Thus, in this work we refer to these geological structures without making a distinction between seismogenic sources and faults. In detail we use DISS seismogenic sources to infer the most likely kinematics of

any CPTI15 earthquake and populate three subcatalogues: one for extensional faulting (EF), one for compressional faulting (CF) and one for strike-slip faulting (SS).

The main weakness of DISS rests in its poor resolution of the slip rates, which tend to be elusive and speculative for almost all sources with very few exceptions (e.g. the data supplied to DISS by Kastelic & Carafa (2012); Maesano *et al.* (2013), and Maesano *et al.* (2015)). Indeed the geometry, location and state of activity - and occasionally even the kinematics - of some DISS seismogenic sources are challenged by other scientists (e.g Aloisi *et al.* 2013; Carannante *et al.* 2015). To address this circumstance in Section 4 we show that the potential mislocation of a DISS fault has a marginal impact on our method of assigning a CPTI15 earthquake to the appropriate subcatalogue. Furthermore, we show that DISS-predicted and observed focal mechanisms exhibit relatively small differences. Prior to beginning our calculations we excluded the ITCS027 "Bore-Montefeltro-Fabriano" seismogenic source (http://diss.rm.ingv.it/diss/), a laterally-continuous thrust front extending from the southern Marche to the Po Plain over a distance of nearly 400 km. The compilers of the DISS database contend that some historical earthquakes, and specifically the *m*6.2, 3 June 1781 Cagli earthquake, occurred in the mid-to-lower crust within this compressional seismogenic source (Finetti *et al.* 2001; Lavecchia *et al.* 2003). We do not question this assignment, yet we believe that such a long seismogenic source is unlikely to be continuous, considering the rheology of the lower Adriatic crust (a mixture of predominantly-plastic, locally-brittle: Carafa & Barba, 2011), and may hence introduce a bias in the process of assigning CPTI15 earthquakes to faults.

Exactly 112 seismogenic sources fall in the region bounded by green polyline of Figure 1: 57 are compressional faults, 30 are normal faults and 25 are strike-slip faults. The average fault-to-$\hat{\varepsilon}$ angles shown in Table 1 (and used in equation 9) are based on mean fault dips for the EF and CF classes; however, for the SS class this angle is unrelated to fault dip, and so we take both θ_1 and θ_2 as the average of the corresponding angles for the EF and CF classes.

3.4 Long-term deformation model

Determining long-term strain rates in the lithosphere is fundamental for properly calculating the seismic coupling and the coupled thickness. These estimates cannot be obtained easily using the DISS database because this compilation does not consider aseismic deformation or seismogenic sources below $m = 5.5$. Also large-scale tectonic models (e.g. Carafa *et al.* 2015) currently lack the resolution needed to calculate the long-term tectonic moment rate for each faulting class. A sound alternative is to use the moment rate determined from GPS-derived strain rates, but these are far from being representative of long-term deformation pattern in Italy without first discounting the short-term transients, as shown by Carafa & Bird (2016). These investigators have recently determined the long-term deformation patterns for Italy, after anticipating and discounting short-term transients in GPS data, and also after including in their kinematic modeling the azimuths of most-compressional principal horizontal stresses. Independent datasets on active faulting and earthquake kinematics suggest that these steps are both necessary to produce credible long-term strain-rate maps. However, some degrees of uncertainty remain in the selection of a single preferred model. Thus, we calculate the diffusivities for the three classes (CF, EF and SS) using all models with $12 \cdot 10^8$ m^2 < A_0 < $^{22 \cdot 10^8}$ m^2 of Experiment 3 discussed in Carafa & Bird (2016) (Table 2). Using this procedure we aim to capture the epistemic uncertainty in the estimation of the long-term strain-rate (Figure 2). Admittedly, the long-term models of Carafa & Bird (2016) yield strain rates which may be either elastic, permanent, or mixed because they are based on GPS strain rates whose character is uncertain. The elastic rebound theory, however, suggests that the spatial separation between sites experiencing elastic strain accumulation and non-elastic permanent strain may be as little as a few kilometers or tens of kilometers. Also, it is not practical to attempt to correct observed strain rate fields to an

idealized long-term equivalent when dealing with deformation models that do not include faults. Therefore, we follow Bird & Kreemer (2015) in assuming that modeled long-term strain rates can be used as proxies for long-term permanent strain rates. Any errors introduced by this assumption will only affect the specific forms of local maxima, but not the overall regional total strain or seismicity.

4. Classification of CPTI15 earthquakes and apparent fault half-width derived from the DISS database

Our method for assigning earthquakes from the CPTI catalog to DISS faults follows Bird & Kagan (2004) in its three-step method and Bayesian philosophy. In the first step, we make a prior assumption that a single earthquake has been generated by each DISS fault, in turn, and compute a set of maps of the probability densities that the epicenter has various possible locations near the fault trace (and perhaps, a limited range of focal mechanisms). In the second step, we make a different prior assumption: that a particular historical earthquake was generated by one of these DISS faults. The ratios of probability densities computed in the first step are then scaled (also considering relative fault activity) to be absolute probabilities that each of the faults was the source. In a few cases where all probability densities are zero, we will reject the prior assumption, and the earthquake will remain unclassified. In those cases where we can proceed to the third step, we will assign the historical earthquake to the most likely causative fault, using either a maximum-probability criterion or a Monte-Carlo method, based on the absolute probabilities computed in step 2. Once the earthquake is assigned to a fault, it will take its tectonic class assignment (EF, CF, or SS) from the known rake of that fault.

Using the symbol "*E*" for "an earthquake" and "*F*" for "a fault", Bayes theorem states that:

$$P(F \mid E) = P(E \mid F) \times P(F) / P(E) \quad (12)$$

The goal is to compute $P(F \mid E)$ for every fault, for every historic earthquake, so that we will be able to perform step 3 and assign that earthquake to a fault. In Step 1 we will estimate the fault-specific terms $P(E \mid F)$ and $P(F)$. The term $P(E)$, which is the spatial (and perhaps orientation) field of prior probability densities for the next new earthquake (independent of the fault database), could be determined from seismicity data, but actually this is not necessary; in step 2 we will assume that the sum of probabilities $P(F \mid E)$ over all faults equals unity (for each historical earthquake), and thus the value of the common factor $P(E)$ will not be needed.

The first step is to map the conditional probability densities that a particular epicenter will be generated by a particular fault when it generates its next earthquake. An important technical aspect to face is the variable digitization style of fault traces in the DISS database. Each active fault is represented in DISS by a series of spatial steps with different lengths, and computing the probability densities for each fault-step would not be independent of its length. In order to avoid such a bias we compute the map of probability densities (of alternative epicenters) for each fault as a whole, summing over its digitization steps. This method gives results that are (nearly) independent of the size of the digitization step.

The probability density $P(E \mid F_i)$ that fault i, digitized in N steps, generates its next earthquake with any potential epicenter (θ, ϕ) is assumed to have this form:

$$P(E / F_i) = \sum_{n=1}^{N} X_n(f_n(\theta,\phi))Y_n(s_n(\theta,\phi)) . \quad (13)$$

where X is a cross-strike probability density function, θ and ϕ are the latitude and the longitude of the possible earthquake, f is the offset of the epicenter from the peak of the seismicity distribution of the n-th step, Y is an along-strike probability density function, and s is a local variable expressing the position along a horizontal axis parallel to the step.

To prepare for the assignment of earthquakes which have known focal mechanisms (which are only the most recent ones), we also use an alternative form that includes the probability densities (in orientation space) of resulting earthquakes with a particular triplet of principal-axis orientations, Q .

$$P(E \mid F_i) = Q \times \sum_{n=1}^{N} X_n(f_n(\theta,\phi))Y_n(s_n(\theta,\phi)) . \quad (14)$$

The cross-strike probability function X_n is defined as

$$X_n = \begin{cases} \frac{1.0}{0.95} \cdot \frac{\sqrt{2}}{\sqrt{\pi}} \cdot \frac{1}{h_i} \cdot \exp\left[-2 \cdot \left(\mathrm{f}_n / h_i\right)^2\right]; \mathrm{f}_n \le h_i \\ 0 \qquad\qquad\qquad\qquad\qquad\quad ; \mathrm{f}_n > h_i \end{cases} \quad (16)$$

with h_i being the apparent half-width of DISS faults and f_n being the distance measurement between the peak of the map-distribution of historical intensities (a proxy for the epicentroid) and the (model-based) center of the band of seismicity expected from that fault step (not the fault trace). The center of the expected band of seismicity is offset with respect to the fault trace by $0.5 \cdot \left(z_{\text{bottom}} - z_{\text{top}}\right) / \tan\alpha$ on the hanging-wall side of the fault, with α being the fault dip and $\left(z_{\text{bottom}} - z_{\text{top}}\right)$ defining the seismogenic thickness and depth interval of the seismicity associated with the given fault. Here z is measured from the surface near the fault; *i.e.*, it is a depth rather than a negative elevation. Note that h_i is a hard threshold beyond which this fault cannot generate any earthquakes.

Bird & Kagan (2004) empirically determined the apparent boundary half-width h_i of each plate boundary class. Their estimates varied between 128 km for Oceanic Transform Faults to 257 km for Continental Transform Faults. In detail this half-width incorporated the effects of four spatial dimensions: (*i*) the half-width of the set of fault traces approximated as a single boundary step at the surface; (*ii*) the half-width added by the dip of each fault, if that fault is not vertical; (*iii*) the error in the mapped position of each plate boundary; (*iv*) the earthquake mislocation. For regional or national-scale databases like DISS the apparent fault half-widths h_i are expected to be smaller, yet they need to be reassessed. Thus we tentatively inferred dimensions (*i*)-(*iv*), in some cases speculating, in others using well-known patterns.

For our project the uncertainties on strike and dip of each seismogenic source reported in DISS yield a good proxy for dimension (*i*) of Bird & Kagan (2004). Considering both uncertainties the projection of the fault plane onto the Earth surface yields (*i*) in the range 3-8 km.

Dimension (*ii*) of Bird & Kagan (2004) (half-width added by fault dip) is generally accurate in DISS: the fault geometry at depth is carefully determined through a combination of different lines of evidence ranging from field geology to oil exploration observations to focal mechanisms. On average

dimension (*ii*) is expected to be 10 km for compressional faults, 6.5 km for extensional faults and 4 km for strike-slip faults.

In a few cases the coseismic rupture coincides with the surface trace of a DISS seismogenic source; more frequently the seismogenic source is blind and is expected to extend upward into different splays from its shallowest tip. A somewhat similar reasoning can be applied for the prolongation of well-defined surface splays; it is rather unlikely that they converge into a single, perfectly-planar fault at depth. Thus, we speculate that a realistic mislocation of seismogenic sources (dimension (*iii*) of Bird & Kagan 2004) around 1-5 km can be taken into account without underestimating the information content of the DISS database. Nevertheless, we can dismiss major errors in the mapped position of each fault. The compilers of the DISS database hold a significant expertise in georeferencing data of different nature. Furthermore, this database collects all the information that is available in the literature and it is unlikely that some badly mislocated fault would enter the published seismogenic source without any further inspection.

Dimension (*iv*), that is the mislocation of an historical earthquake, is the hardest to determine. Spatial and temporal variability of historical sources, and also the location algorithm, are known to bias the true epicentral location. To estimate the extent of this mislocation we compared the epicentroids of different earthquakes reported in both the CPTI04 (an earlier version of CPTI15) and CPTI15 (Rovida *et al.* 2016) catalogues. We find that the largest discrepancy is found in the epicentroids assigned to the 23 February 1818 event, presumably located offshore, with the two locations differing by 29 km. Similar mislocations may affect other coastal or offshore earthquakes (22 October 1919, M_w 5.2 Anzio earthquake; 16 August 1916, M_w 5.9 Alto Adriatico-Rimini earthquake), but we do expect better precision on land. Therefore, we suggest that dimension (*iv*) is between 5 and 30 km.

Combining the four characteristic dimensions gives 15-50 km as the expected range of *a priori* apparent half-width h_i of DISS faults.

The factor $Y_n(s_n(\theta,\phi))$ is a function of distance s along the length of the trace, which expresses the position along a horizontal axis parallel to the fault trace. Earthquakes actually caused by a particular step on a given fault might appear beyond the ends of the step due to along-strike mislocation and/or earthquake location error (see dimensions (*iii*) and (*iv*) discussed above). The combination of these errors are not expected to exceed 5-20 km, a quantity that we define as 2σ. Following Bird & Kagan (2004) we use the product of two normal cumulative distribution functions to produce a smoothed boxcar probability density function

$$Y_n\left(s_n\left(\theta,\phi\right)\right) = c\left[\int_{-\infty}^{s} e^{-s'^2/2\sigma^2} ds'\right]\left[\int_{-\infty}^{s} e^{-(s'-l_n)^2/2\sigma^2} ds'\right] \quad (17)$$

where c is computed so that $\int_{-\infty}^{\infty} Y_n(s)ds = 1$.

In cases where we will be comparing a known focal mechanism to the expected focal mechanism (for each fault), factor Q is also needed to express the likelihood of different rupture mechanisms associated with the given fault. We make the simplifying assumption that the ratios of angular probability densities Q that should be compared to a given real earthquake can be expressed as a function of only one variable: the minimum three-dimensional rotation Φ necessary to make the principal axes of the expected earthquake (based on fault strike, dip and rake angles) coincide with the actual earthquake focal mechanism (Kagan, 1991). In detail, we define

$$Q(\Phi) = \frac{3}{2\Phi_m} \begin{cases} 1 - (\Phi/\Phi_m)^2; & \Phi \le \Phi_m \\ 0; & \Phi > \Phi_m \end{cases} \qquad (18)$$

This will ensure that an earthquake is not assigned to a fault with an incompatible sense of slip. The main cause of unexpected directions of moment tensor axes is the apparent low friction of some active faults. To avoid that one might choose $\Phi_m = 45°$. However, Bird & Kagan (2004) suggested to use $\Phi_m = 60°$ because moment tensors in each catalogue may be rotated from the true mechanisms by median amounts of about 15° (Kagan 2003).

In the previous equations we estimated $P(E|F)$, which is a unit-dependent probability density. The factor $P(E)$ is also a probability density in the same units. These units depend on whether alternative focal mechanisms are considered, as in (14), or neglected, as in (13). It remains to estimate $P(F)$ for each fault, which is the probability that the next shallow earthquake in the region will be caused by that fault. $P(F)$ is assumed to be proportional to the along-fault sum of factors A_n, which are the numbers of detectable earthquakes occurring on step n, assumed to be composed of a tectonic regime factor and a length factor:

$$A_n = C_{\text{class}} \frac{l_n}{L_{\text{class}}} \qquad (15)$$

with C_{class} being the number of earthquakes produced by faults of class CF ($\text{class} = 1$), EF ($\text{class} = 2$) and SS ($\text{class} = 3$), l_n is the trace length of step n and L_{class} is the total trace length of all steps in the considered class. The counts C_{class} are determined by boot-strap iteration because some earthquakes fall at almost equal distance from the extensional and compressional faults; some information on the average behavior of each class may hence support the assignment of each event to the relevant class. C_{class} is rapidly stabilized by iteration; Table 1 reports the final values of $\frac{C_{\text{class}}}{L_{\text{class}}}$.

Compared to the method of Bird & Kagan (2004) our A_n values do not include any fault slip rate factor, because in DISS the slip rate is usually the most volatile and poorly-constrained parameter. However, we acknowledge that what seems to be a class factor could really be influenced by unknown slip-rate factors. Should slip rates be determined more accurately in the future, it will always be possible to look back and re-evaluate this issue.

We computed cumulative distributions in the 10-50 km range for h_i and 0-30 km range for 2σ to determine their final values. The selection of preferred values for h_i and 2σ involves a compromise between two conflicting considerations. First, it is fundamental to associate the largest possible amount of seismic moment and the largest number of earthquakes with known faults. Second, h_i should not be larger than 40-50 km because that is on average the spatial separation between zones undergoing extension and zones undergoing compression in the Apennines. Doing otherwise would inevitably cause an increasing interference among seismogenic sources with opposite kinematics. Figure 3 shows that $h_i - 2\sigma$ coupled with $h_i \ge 25$ km and $2\sigma \ge 10$ km allows us to assign > 90% of CPTI15 earthquakes to DISS faults and to recover nearly all the seismic moment (>95%).

Thus, we set $h_i = 25$ km and $2\sigma = 10$ km for the 346 earthquakes with $m \ge 4.8$ selected from the CPTI15 catalogue (starting with the year 1880), resulting in 134 earthquakes assigned to the CE class,

140 to EF and 40 to SS (Figure 4). Figure 3 shows the cumulative distribution of peak probabilities $P(F_i \mid E)$: out of 314 earthquakes assigned to faults, 228 were assigned with a peak probability equal to 1.0, while for 280 events the probability is 0.9 or larger. For 32 earthquakes, however, we could not determine the causative faults. This occurs when earthquakes fall too far from any DISS fault. We assigned these 32 events to the three classes, proportionally to their populations, resulting in 13.7, 14.3 and 4.1 additional, kinematically undetermined earthquakes for CF, NF and SS respectively.

It could be argued that the absence of focal mechanisms for nearly all earthquakes in the CPTI15 catalogue may result in an unbalanced and decisive role of the fault kinematics adopted in the DISS database: an incorrect rake assignment for a DISS fault would result in a wrong class assignment for all associated CPTI earthquakes. To dispel these doubts we performed a double-blind experiment. We first selected the $m \geq 5$ events with depth ≤ 25 km from the recently-published database of focal mechanisms of Montone & Mariucci (2016). Then, in the first experiment we assigned earthquakes to faults using the observed focal mechanisms (equations (14, 18), using factor Q), while in a second experiment we used (13). We found that 11 out of 76 earthquakes were unassigned to faults in the first experiment, while in the second experiment the unassigned earthquakes dropped to only 6. Furthermore the 65 earthquakes assigned to faults in both the first and second experiment do not change their most-probable causative fault kinematics. This test suggests that our method of classifying earthquakes is rather stable, and that the absence of focal mechanisms for CPTI15 earthquakes is not a severe limitation for recovering their tectonic regime from DISS faults, as long as such faults fit the observed focal mechanisms. We tested this conclusion by further investigating the misfits between the expected focal mechanisms (based on the strike, dip and rake of the DISS faults) and the observed ones for the 71 events assigned to a DISS fault in the second experiment. Figure 3 shows the cumulative distribution of focal mechanism misfits in a format similar to an error-diagram display (Kagan 2009; Kagan & Jackson 2015). We find a fairly good agreement between the observed kinematics and the predictions of the DISS database: 80% of events exhibit a misfit <45°, estimated as the maximum rotation of a double-couple source (Kagan, 1990) between that predicted by DISS and the real focal mechanism.

5. Seismicity parameters

5.1 Tapered Gutenberg-Richter distributions

Once the three subcatalogues were populated we sought to determine the maximum-likelihood estimates of β and M_c to calculate $\dot{M}_{\text{seis}}$(equation 3). The number of earthquakes and their magnitude distribution for the SS subcatalogue, however, is insufficient to obtain a stable result; thus we dismissed this subcatalogue as unsuitable for (β, M_c) estimation. The location of these faults in the DISS database, all lying in the Adriatic foreland next to thrust faults, suggests that a common geological settings could result in similar values for Gutenberg-Richter parameters between these two classes. Based on this reasoning we merged the CF and SS subcatalogues for purposes of estimating their common Gutenberg-Richter parameters. This combined CF-SS subcatalogue is used only for the determination of β and M_c, whereas for $\dot{M}_{\text{seis}}$ estimations the earthquakes in each subcatalogue are kept separate.

An easy and convenient way to visualize the likelihood estimates for each (β, M_c) combination is a contour map of log-likelihood relative to the local peak with respect to the two parameters (Figure 5). For the investigated time interval (1880-2013) the EF and CF-SS contour maps have a zero contour line that is open to infinity in the M_c direction. This means that all catalogues lack the minimum

number of large earthquakes that are needed for a purely statistical maximum-likelihood estimate of the 95%-confidence upper-bound on M_c. In a relatively slow-deforming region such as Italy, where the historical earthquake record extends far back in time, it is appropriate to investigate longer time intervals so as to capture more large events and constrain M_c more effectively. To this end we extended all three subcatalogues using different threshold magnitudes along with the historical completeness bounds reported in Stucchi *et al.* (2011). In detail, we included all earthquakes that occurred after 1786 with $m_t = 5.22$ for EF and 1700 for CF-SS. In this conditional case, we assumed that the β values of all extended catalogues are more uncertain than those obtained in the time span 1880-2013. Therefore we fixed β at the 1880-2013 value and defined M_c as the value associated with the highest likelihood occurring in the corresponding column of the (β, M_c) contour grid.

Table 1 shows the 95% confidence level on M_c estimations. A question mark next to a parameter indicates that we could not determine the upper limit for that parameter. For each class we also reported the final estimates of the total seismic moment rate $\dot{M}_{seis}$ which was used for $\langle cz \rangle$ calculations (denominator in equation 11).

5.2 Shear modulus estimates and coupled thickness

The value of the shear modulus used for estimating tectonic moment rates is often taken from a global Earth model (e.g. PREM or CRUST). However, the shear modulus is a variable function of depth and location (Bressan *et al.* 2012), and problems with the consistency of global estimates may arise. Alternatively, the shear modulus can be calculated using the relationships between the elastic moduli and density and seismic velocities V_p and V_s (Bressan *et al.* 2012). Di Stefano & Ciaccio (2014) recently published a set of three-dimensional seismic tomography models beneath Italy, while several gravity models of the upper crustal layers have been produced for different parts of Italy (e.g., Improta *et al.* 2003; Tiberti *et al.* 2005), the prevalent rocks-types being limestones/dolostones of the carbonate platforms and the Paleozoic crystalline basement. Thus, we decided to determine μ using available regional S- velocities and densities rather than assuming global averaged values.

In detail, Di Stefano & Ciaccio (2014) computed travel-times and ray paths of refracted seismic waves using the Moho discontinuity obtained by Di Stefano *et al.* (2011). Then, seismic velocity values were assigned and modified on a 15 × 15 × 15, 3D grid of nodes with layers having their bottoms at 8, 22, 38, 52, 66, and 80 km depth. For the present work we are most interested in the values obtained for the first two layers where nearly all m>5 earthquakes occur. We found V_p = 6,018 m/s (RMS=332 m/s) for the 0-8 km layer and V_p = 7,076 m/s (RMS=415 m/s) for the 8-22 km layer. The ratio V_p/V_s = 1.82 is almost constant in both layers, while we set the averaged upper crustal densities to $\rho = 2670 \pm 70$ kg/m^3 (Improta *et al.* 2003; Tiberti *et al.* 2005). The resulting values are $\mu_{min} = 2.92 \cdot 10^{10}$ Pa for the uppermost layer and $\mu_{max} = 4.06 \cdot 10^{10}$ Pa for the deeper layer, which represent the bounds of the μ interval to be used for the upper crust in Italy.

Once the shear modulus has been calculated, having already determined for each class the total seismic moment rate $\dot{M}_{seis}$ (Table 1) and the diffusivity in all long-term deformation models (Table 2), we applied equation (11) to calculate the average coupled thickness $\langle cz \rangle$ for each of our three fault

classes (Table 1). The coupled thickness estimates are 3.8, 7 and 5 km for CF, EF and SS, respectively. The coupled thickness ranges for EF and CF are open to future improvements; according to Kagan (2014) a correct estimation of the coupling *c*, and consequently of the coupled thickness $\langle cz \rangle$, depends on the number of earthquakes above the threshold magnitude but also on the magnitude difference $\Delta m = m_c - m_t$. In this work we used $m_t = 4.8$ and determined $m_c \cong 7$, resulting in $\Delta m \simeq 2$. Hence, a regular seismic moment rate release - that is to say, a good match between long-term estimates and short-term observations - should be expected only after accumulating at least 350-400 earthquakes for each subcatalogue (Kagan, 2014). For the past 135 years the number of earthquakes above $m_t = 4.8$ in each subcatalogue is less than 200, resulting in an "irregular" seismic moment release distribution for the whole of Italy. Consequently, any $\langle cz \rangle$ estimation for Italy, including ours, must face this limitation in the number of earthquakes that appear in the earthquake catalogue starting from the year 1880. We could use longer time intervals, but this would require setting larger threshold magnitudes (see Stucchi *et al.*, 2011); this would not help because the number of known earthquakes above any threshold magnitude drops exponentially and it never equals the number of earthquakes required by Kagan's (2014) formulation for a stable estimation of *c*. Furthermore, we cannot rule out that the long-term deformation models used in this work are still partially contaminated by short-term geodetic transients, whose net effect is to reduce the estimated $\langle cz \rangle$, especially for the EF. For instance, we may suspect that the long-term strain rates of the Southern Apennines are still partially affected by the postseismic relaxation following the *m* 6.9, 23 November 1980, Irpinia earthquake.

Nevertheless, we wish to point out that estimating the coupled thickness, which is the seismogenic thickness multiplied by the seismic coupling, allows us to overcome the problem of keeping the seismogenic thickness separated from the seismic coupling, returning a realistic product of these two parameters even though each of them is inherently uncertain. Referring to the coupled thickness estimates is helpful to avoid falling into wrong deductions. For example, D'Agostino (2014) calculated GPS-derived moment rates and compared them to seismicity rates, claiming that in the Southern Apennines all GPS-recorded deformation is released by earthquakes (i.e. $c \simeq 1$). The author used an *a priori* seismicity cutoff ($z = 10 \pm 2.5$ km), so the actually calculated coupled thickness was $7500 < \langle cz \rangle < 12500$ m. The Southern Apennines are undergoing extension and most of the earthquakes that occurred in this region fall into the EF class. Consequently, the coupled thickness interval that we can derive from the results of D'Agostino (2014) is in good agreement with our estimate for EF class because they overlap in a large range. However, we disagree with the statement that $c \simeq 1$ for the Southern Apennines. Over the time interval spanned by the GPS measurements reported in D'Agostino (2014) significant microearthquake activity has been recorded in this region up to 15 km depth (e.g. De Matteis *et al.* 2012; Matrullo *et al.* 2013), hence not only in the uppermost 10~12.5 km of the crust. We contend that the *a priori* assumption by D'Agostino (2014) of a seismicity cutoff at 10 km affects the finding that $c \simeq 1$; using the observed seismicity cutoff ($\simeq 15$ km) we would obtain a ~30% smaller *c*. Because the depth of the seismicity cutoff is independently and reliably determined for the Southern Apennines, this represents a fortunate opportunity to unmask a biased seismic coupling estimate deduced from a correct coupled thickness calculation. This represents the main reason to estimate $\langle cz \rangle$ rather than reporting less-reliable estimates of the seismic coupling heavily relying on an assumed – not observed - seismicity cutoff.

6. Seismicity parameters for different fault classes: earthquake forecasts and seismic hazard implications for Italy

We computed forecast maps of the long-term density of earthquake epicenter rates (in m^{-2} s^{-1}) for shallow earthquakes above a forecast threshold magnitude m_f. Except for an adaptation to Italy of fault angles and seismicity coefficients (Table 1), the method generally follows that proposed by Bird & Liu (2007), Bird *et al.* (2010), and Bird & Kreemer (2015). For simplicity we describe the calculation only for a single grid-point falling into one particular finite-element of the long-term deformation model; in this small domain all parameters can be approximated as laterally constant. Hence to forecast seismicity for one grid cell:

(1) the principal axes and principal values of the long-term strain-rate tensor are computed and labelled as in equations (4-6);

(2) based on the orientation and relative magnitude of the principal axes and values, the given grid cell is characterized by a certain amount of strain-rate of class CF or EF and/or SS;

(3) the tectonic moment rate of that grid cell is computed from the long-term permanent strain-rate by equation (10) using the coupled thickness, the elastic modulus and the θ angle for the relevant tectonic class;

(4) the tectonic moment rate of the grid cell is expresses as a (small) fraction of $\dot{M}_{seis}$ of the appropriate subcatalogue(s);

(5) the forecast earthquake rate of the given grid cell (for shallow earthquakes above the subcatalogue threshold m_t) is obtained by multiplying this small fraction by the total earthquake rate in the relevant subcatalogue;

(6) the forecast rate is scaled from the subcatalogue threshold m_t to desired forecast threshold m_f through equation (3), using the beta and the corner magnitude previously estimated for the relevant tectonic class.

The resulting earthquake rates forecasts for m>5.5, m>6.0, m>6.5 and m>7.0 are shown in Figure 6. The Apennines chain, which falls almost completely in the EF class, exhibits the largest seismicity rates for all magnitude bins in our study area, in agreement with the distribution of seismicity reported in CPTI15. Among areas undergoing compression (CF class), the Eastern Alps and the Po Plain show the largest seismicity rates (see Figure 4). Notice that the different values of m_c and β imply for larger magnitudes an increasing ratio between the number of earthquakes respectively predicted for the EF zones and for the CF-SS zones. Earthquakes above m>7.1 were reported for EF faults, but their occurrence is very unlikely in regions falling in the CF and SS classes. Although our maximum-likelihood tests did not completely exclude $m_c > 7.1$ from the tests run for the CF class, we maintain that several independent geological indications support our results. In detail, the faults of the CF class are hosted in highly heterogeneous rock complexes that are part of arc-shaped and highly segmented structures: these are unlikely to allow a seismic rupture to propagate for tens or hundreds of kilometers, thus preventing the generation of large earthquakes. We cannot completely rule out a catastrophic scenario of a rupture jumping across adjacent compressional faults and generating a large ($m > 7.1$) earthquake, but based on geologic and structural evidence we simply consider it very unlikely in the specific compressional settings of our study area.

Our deterministic method to assign each earthquake to its causative fault is based on the highest (peak) probability $P(F_i \mid E)$ (equation 12). The resulting cumulative density function (CDF) of these peak probabilities shows that 78 per cent of them are larger than 0.99, indicating that the majority of earthquake assignment to faults is unambiguous. However, it is always possible that lower peak probabilities could be marginally higher than the probabilities of adjacent faults; in this case the ambiguity in the assignment would not be captured by our method and the uncertainty in the assignment might affect also the coupled thicknesses. To investigate the effect on coupled thickness estimations for the remaining 23% of earthquake assignments that exhibit a peak probability smaller than 0.99 we randomly assigned earthquakes to one of the faults having a positive value of $P(F_i \mid E)$. In detail, we generated a random number, compared it to the three selection bins (one for each class) having a width proportional to their own sums of $P(F_i \mid E)$, and assigned the earthquake to the bin including the random number. We computed several realizations using different seeds for the random-number generator, and found an average variation of four earthquakes for each class. None of the earthquakes with m>6.2 was assigned to a different fault class in any realization, suggesting that this residual uncertainty can be considered marginal in the calculation of the seismic moment rate $\dot{M}_{\text{seis}}$ and of the coupled thickness.

Furthermore, using the maximum-likelihood method we determined different β values for the CF-SS classes with respect to the EF class, supporting the hypothesis of beta varying systematically for different styles of faulting (Schorlemmer et al., 2005). Our results, however, show β values for extensional faulting to be smaller than for compressional faulting in Italy, which is the opposite of what has been found on global scale by Schorlemmer *et al.* (2005). Notably, the null hypothesis of a single β value for the whole of Italy cannot be rejected because the two β ranges for CF-SS and EF (Figure 5) define a largely overlapping interval of β values. In any case, as suggested by Kagan (2014), using different β values resulting from regional earthquake catalogs may still be the best choice, especially if seismicity forecasts are to be prospectively tested using the same catalogs, as it is usually done in CSEP (Schorlemmer et al., 2007; Schorlemmer et al., 2010; Zechar et al., 2010).

Similarly to what we have found for β values, we want to highlight the significant difference of the estimated coupled thickness of the EF and CF classes with respect to global averages of continental plate boundaries. According to the classification of Bird & Kagan (2004), updated by Bird et al. (2009), the global analog for our CF class is the "slow Continental Convergent Boundary" (slow CCB), while the "Continental Rift Boundary" (CRB) is the analog for the EF class (Bird & Liu 2007; Bird & Kreemer 2014, 2015; Bird *et al.* 2015). The $\langle cz \rangle$ of slow-CCB in Bird *et al.* (2009) is 10,900 m, well above the seismogenic thickness $\langle cz \rangle$ determined in this work for the Italian CF class. Also the global average of $\langle cz \rangle$ for CRB (3,000 m) is significantly lower than our estimates of $\langle cz \rangle$ for the Italian EF class. The lower coupled thicknesses for CF and SS in Italy may be attributable to lower corner magnitudes, which result from lower peak magnitudes (for these tectonic classes) in Italy. In contrast, the higher coupled thickness for EF in Italy is not a corner-magnitude effect, as our Italian corner magnitude is actually slightly less than that of the global analogue. We think that both extensional and compressional faulting in Italy reflect a tectonic setting that is specific to this portion of the Mediterranean, and hence the coupled thicknesses (and seismic couplings) we obtain are different from global analogs. For instance, in the most external portions of the active accretionary wedges encircling the Italian peninsula, where many active compressional faults have been mapped, the seismicity record is poor, if not totally silent (see Figure 4). It could be argued that the historical catalogue is prone to miss earthquakes occurring in the open sea; but some compressional areas do

show a reliable and rather long record of past earthquakes, such as the Po Plain in northern Italy, and yet even in these regions the observed seismicity is a small fraction of what would be expected assuming a fully seismic behavior of the active faults. Nevertheless it is wise to be cautious: having determined a limited coupled thickness (or seismic coupling) for areas undergoing compression should not lead anyone to conclude that faults of the CF class do not pose a significant hazard. The coupled thickness/seismic coupling is estimated as an average over large crustal regions, and a low thickness/coupling should not be interpreted without appropriate consideration of the significant variability of the seismic behavior of compressional faults, even at local scale. With respect to this variability we wish to stress that compressional earthquakes tend to occur only where previous tectonic histories have caused more competent rocks such as limestones and dolostones to be placed at depth ranges that are typical of these events, such as the interval 3-10 km (see Bonini *et al.* 2014). If anything, detecting a low thickness/coupling in a region that has experienced large earthquakes, even very infrequent ones, should motivate more detailed work to allow faults that are more likely to exhibit brittle behavior to be singled out (Burrato *et al.*, 2001; Mucciarelli *et al.*, 2015; Tarabusi & Caputo 2016).

From a more general perspective it should be recalled that the thick evaporite formations encircling the Italian peninsula along the external margin of the Apennines chain are effective impermeable seals which control the escape of fluids from beneath, thus potentially increasing local fluid pressures. Once a subduction zone slows down or stops moving, as the Gibraltar and Calabrian arc/Apennines arcs have done in the recent geological past, these super-hydrostatic pore pressures should leak away slowly, at least in principle, but we do not know how long this process takes. This high pore pressure in the forearc areas, like the Apennines (EF faults), reduces the shear stress necessary for frictional sliding. In addition to that, the Apennines (and in general the Mediterranean forearcs of subduction zones) exhibit an unusually low heat-flow (*e.g.*, 35-60 mW/m^2), comparable only to the least radiogenic parts of the old shields (Baltica, Laurentia). The combination of these high pore pressures, high strain rates and low temperatures is likely to cause the critical brittle/ductile transition depth (for any local rheology) and the related seismicity cutoff to be deeper than normal. From a rheological perspective the main consequence of these circumstances is that brittle deformation is encouraged to continue to greater depth because temperatures are still too low to deform the upper crust by ductile creep, and effective pressures are too low to impose plastic behavior. A deeper brittle/ductile transition implies a higher $\langle cz \rangle$ value resulting from the complex interaction of high pore pressure, of the widespread occurrence of evaporites and of the presence of a subduction in its final stage. This is indeed the current condition of most, if not all, EF faults in the Apennines.

7. Conclusions

Over the past few years several investigators have started developing long-term tectonic models aimed at constraining seismicity and seismic hazard forecasts for the densely inhabited central Mediterranean region. For Italy these models follow a promising avenue, thanks to the availability of rich, reliable and regularly updated seismogenic fault and historical earthquake databases and to the density of permanent GPS stations. On these grounds we thought it would be useful to construct, test and discuss an objective and reproducible algorithmic path to forecast seismicity in Italy, following rules and practices that are meant to avoid methodological errors in calculating earthquake forecasts from long-term deformation models. In detail we have determined beta, M_c (and thus m_c), and the coupled thickness (seismogenic thickness times seismic coupling) separately for compressional, extensional and strike-slip faults. Our findings can be used across the central Mediterranean to forecast seismicity using long-term deformation models or fault databases. Finally, we have forecast and made available long-term seismicity forecast maps for the Italian Peninsula, which can be tested during future decades and centuries.

Our work was meant to address the role of seismic coupling in controlling estimates of seismic hazard based on tectonic and fault data. We have shown that assuming that the seismic coupling equals unity for all fault systems may overestimate the seismic hazard for all fault zones, particularly those accommodating compression. For these areas we point out the difficult balance one has to strike between resorting to geodetic data and/or active faulting evidence to overcome possible – and in fact well-known – limitations of the earthquake record, and overemphasizing the role of active faults. In this work we have suggested a strategy to avoid an unwarranted use of any of these sources to assess the regional seismic hazard; an overestimation of the local earthquake potential could fatally harm the economy of portions of Italy that are densely inhabited, host significant industries and infrastructures, and are the locus of hydrocarbon exploitation, such as the Po Plain, the Romagna-Marche-Abruzzo coast and the Adriatic offshore.

References

Albarello, D., Camassi, R. & Rebez, A., 2001. Detection of space and time heterogeneity in the completeness of a seismic catalog by a statistical approach: an application to the Italian area, *Bulletin of the Seismological Society of America*, 91, 1694-1703, doi: 10.1785/0120000058.

Aloisi, M., Bruno, V., Cannavò, F., Ferranti, L., Mattia, M., Monaco, C. & Palano, M., 2013. Are the source models of the M 7.1 1908 Messina Straits earthquake reliable? Insights from a novel inversion and a sensitivity analysis of levelling data, *Geophys. J. Int.*, 192(3), 1,025-1,041, doi: 10.1093/gji/ggs062.

Bakun, W.H. & Wentworth, C.M., 1997. Estimating earthquake location and magnitude from seismic intensity data, *Bulletin of the Seismological Society of America*, 87, 1502-1521.

Barba, S., Carafa, M.M.C., Mariucci, M.T., Montone, P. & Pierdominici, S., 2010. Present-day stress-field modelling of southern Italy constrained by stress and GPS data, *Tectonophysics*, 482, 193-204, doi: 10.1016/j.tecto.2009.10.017.

Basili, R., Valensise, G., Vannoli, P., Burrato, P., Fracassi, U., Mariano, S., Tiberti, M.M., & Boschi, E., 2008. The database of individual seismogenic sources (DISS), version 3: Summarizing 20 years of research on Italy's earthquake geology, *Tectonophysics*, 453, 20-43. doi: 10.1016/j.tecto.2007.04.014.

Becker, D. & Meier, T., 2010. Seismic slip deficit in the southwestern forearc of the Hellenic Subduction Zone, *Bull. Seism. Soc. Am.*, 100(1), 325-342, doi: 10.1785/0120090156.

Bird, P. & Kreemer, C., 2015. Revised Tectonic Forecast of Global Shallow Seismicity Based on Version 2.1 of the Global Strain Rate Map, *Bulletin of the Seismological Society of America*, **105**, 152-166, doi: 10.1785/0120140129.

Bird, P. & Liu, Z., 2007. Seismic Hazard Inferred from Tectonics: California, *Seismological Research Letters*, **78**, 37-48, doi: 10.1785/gssrl.78.1.37.

Bird, P., & Y. Kagan, 2004. Plate-tectonic analysis of shallow seismicity: Apparent boundary width, beta, corner magnitude, coupled lithosphere thickness, and coupling in seven tectonic settings, *Bull. Seism. Soc. Am.*, **94(6)**, 2380–2399, doi:10.1785/0120030107.

Bird, P., Jackson, D.D., Kagan, Y.Y., Kreemer, C. & Stein, R.S., 2015. GEAR1: A Global Earthquake Activity Rate Model Constructed from Geodetic Strain Rates and Smoothed Seismicity, *Bulletin of the Seismological Society of America*, 105**,** 2538-2554, doi: 10.1785/0120150058.

Bird, P., Kagan, Y.Y. & Jackson, D.D., 2002. Plate tectonics and earthquake potential of spreading ridges and oceanic transform faults. *in Plate Boundary Zones* eds. Stein, S. & Freymueller, J. T.

Bird, P., Kagan, Y.Y., Jackson, D.D., Schoenberg, F.P. & Werner, M.J., 2009. Linear and Nonlinear Relations between Relative Plate Velocity and Seismicity, *Bulletin of the Seismological Society of America*, 99, 3097-3113, doi: 10.1785/0120090082.

Bird, P., Kreemer, C. & Holt, W.E., 2010. A Long-term forecast of Shallow Seismicity Based on the Global Strain Rate Map, *Seismological Research Letters,* 81, 184-194, doi: 10.1785/gssrl.81.2.184.

Bonini, L., Toscani, G., & Seno, S. 2014. Three-dimensional segmentation and different rupture behaviour during the 2012 Emilia seismic sequence (Northern Italy), *Tectonophysics*, 630, 33–42, doi:10.1016/j.tecto.2014.05.006.

Bressan, G., Gentile, G.F., Tondi, R., De Franco, R. & Urban, S., 2012. Sequential Integrated Inversion of tomographic images and gravity data: an application to the Friuli area (north-eastern Italy), *Bollettino di Geofisica Teorica ed Applicata,* 53, 191-212, doi: 10.4430/bgta0059.

Bungum, H., 2007. Numerical modelling of fault activities, *Computers & Geosciences*, 33, 808-820, doi: 10.1016/j.cageo.2006.10.011.

Burrato, P., Ciucci, F., & Valensise, G., 2003. An inventory of river anomalies in the Po Plain, Northern Italy: evidence for active blind thrust faulting, *Ann. Geophys.*, **5**, 865-882, doi: 10.4401/ag-3459.

Burrato, P., Vannoli, P., Fracassi, U., Basili, R., & Valensise, G., 2012. Is blind faulting truly invisible? Tectonic-controlled drainage evolution in the epicentral area of the May 2012, Emilia-Romagna earthquake sequence (northern Italy), *Ann. Geophys.*, 55(4), 525-531, doi: 10.4401/ag6182.

Carafa, M.M.C. & Barba, S., 2011. Determining rheology from deformation data: The case of central Italy, *Tectonics*, 30, doi: 10.1029/2010tc002680.

Carafa, M.M.C. & Bird, P., 2016. Improving deformation models by discounting transient signals in geodetic data: 2. Geodetic data, stress directions, and long-term strain rates in Italy, *Journal of Geophysical Research: Solid Earth,* 121, 5557-5575, doi: 10.1002/2016jb013038.

Carafa, M.M.C., Barba, S. & Bird, P., 2015. Neotectonics and long-term seismicity in Europe and the Mediterranean region, *Journal of Geophysical Research: Solid Earth,* 120, 5311-5342, doi: 10.1002/2014jb011751.

Carannante, S., Argnani, A., Massa, M., D'Alema, E., Lovati, S., Moretti, M., Cattaneo, M., & Augliera, P., 2015. The May 20 (M_w 6.1) and 29 (M_W 6.0), 2012, Emilia (Po Plain, northern Italy) earthquakes: New seismotectonic implications from subsurface geology and high-quality hypocenter location, *Tectonophysics*, **655**, 107-123, doi: 10.1016/j.tecto.2015.05.015.

Cowie, P. A., Scholz, C. H., Edwards, M., & Malinverno, A., 1993. Fault strain and seismic coupling on mid-ocean ridges, *J. Geophys. Res.*, **98 (B10)**, 17,911-17,920.

D'Agostino, N., 2014. Complete seismic release of tectonic strain and earthquake recurrence in the Apennines (Italy), *Geophysical Research Letters,* **41**, 1155-1162, doi: 10.1002/2014gl059230.

De Matteis, R., Matrullo, E., Rivera, L., Stabile, T.A., Pasquale, G. & Zollo, A., 2012. Fault Delineation and Regional Stress Direction from the Analysis of Background Microseismicity in the southern Apennines, Italy, *Bulletin of the Seismological Society of America*, 102, 1899-1907, doi: 10.1785/0120110225.

Devoti, R., Pietrantonio, G. & Riguzzi, F., 2014. GNSS networks for geodynamics in Italy, *Física de la Tierra*, 26, 11-24, doi: 10.5209/rev_FITE.2014.v26.46968.

Di Stefano, R. & Ciaccio, M.G., 2014. The lithosphere and asthenosphere system in Italy as inferred from the Vp and Vs 3D velocity model and Moho map, *Journal of Geodynamics*, 82, 16-25, doi: 10.1016/j.jog.2014.09.006.

Di Stefano, R., Bianchi, I., Ciaccio, M.G., Carrara, G. & Kissling, E., 2011. Three-dimensional Moho topography in Italy: New constraints from receiver functions and controlled source seismology, *Geochemistry, Geophysics, Geosystems*, 12, doi: 10.1029/2011gc003649.

DISS Working Group, 2015. Database of Individual Seismogenic Sources (DISS), Version 3.2.0: A compilation of potential sources for earthquakes larger than M 5.5 in Italy and surrounding areas. © INGV 2015 - Istituto Nazionale di Geofisica e Vulcanologia, http://diss.rm.ingv.it/diss/, doi: 10.6092/INGV.IT-DISS3.2.0.

Field, E.H., Arrowsmith, R.J., Biasi, G.P., Bird, P., Dawson, T.E., Felzer, K.R., Jackson, D.D., Johnson, K.M., Jordan, T.H., Madden, C., Michael, A.J., Milner, K.R., Page, M.T., Parsons, T., Powers, P.M., Shaw, B.E., Thatcher, W.R., Weldon, R.J. & Zeng, Y., 2014. Uniform California Earthquake Rupture Forecast, Version 3 (UCERF3) - The Time-independent model, *Bulletin of the Seismological Society of America,* **104**, 1122-1180, doi: 10.1785/0120130164.

Finetti, I.R., Boccaletti, M., Bonini, M., Del Ben, A., Geletti, R., Pipan, M. & Sani, F., 2001. Crustal section based on CROP seismic data across the North Tyrrhenian–Northern Apennines–Adriatic Sea, *Tectonophysics,* 343, 135-163, doi: 10.1016/s0040-1951(01)00141-x.

Gasperini, P., Bernardini, F., Valensise, G. & Boschi, E., 1999. Defining seismogenic sources from historical earthquake felt reports, *Bulletin of the Seismological Society of America,* 89, 94-110, doi.

Guidoboni, E., Muggia, A, & Valensise, G., 2000. Aims and methods in Territorial Archaeology: possible clues to a strong IV century A.D. earthquake in the Straits of Messina (southern Italy). In: McGuire, B., Griffiths, D., and Stewart, I. (eds.), The Archaeology of Geological Catastrophes, *Geol. Soc. London Spec. Publications*, 171, 45-70.

Howe, T.M. & Bird, P., 2010. Exploratory models of long-term crustal flow and resulting seismicity across the Alpine-Aegean orogen, *Tectonics,* 29, doi: 10.1029/2009tc002565.

Improta, L., Bonagura, M., Capuano, P. & Iannaccone, G., 2003. An integrated geophysical investigation of the upper crust in the epicentral area of the 1980, Ms=6.9, Irpinia earthquake (Southern Italy), *Tectonophysics,* 361, 139-169, doi: 10.1016/s0040-1951(02)00588-7.

Kagan, Y.Y. & Jackson, D.D., 2015. Likelihood analysis of earthquake focal mechanism distributions, *Geophys J Int,* 201**,** 1409-1415, doi: 10.1093/gji/ggv085.

Kagan, Y.Y., 1990. Random stress and earthquake statistics: spatial dependence, doi: 10.1111/j.1365-246X.1990.tb04584.x.

Kagan, Y. Y., 2014. Earthquake size distribution, in Earthquakes: Models, Statistics, Testable Forecasts, John Wiley & Sons, Ltd, Oxford, UK.

Kagan, Y.Y., 2002. Seismic moment distribution revisited: II. Moment conservation principle, *Geophys J Int,* 149, 731-754, doi: 10.1046/j.1365-246X.2002.01671.x.

Kagan, Y.Y., 2009. Testing long-term earthquake forecasts: Likelihood methods and error diagrams, doi: 10.1111/j.1365-246X.2008.04064.x.

Kanamori, H., 1971. Great earthquakes at island arcs and the lithosphere, *Tectonophysics*, 12, 187-198.

Kastelic, V. & Carafa, M.M.C., 2012. Fault slip rates for the active External Dinarides thrust-and-fold belt, *Tectonics,* 31, doi: 10.1029/2011tc003022.

Kastelic, V., Carafa, M.M.C. & Visini, F., 2016. Neotectonic deformation models for probabilistic seismic hazard: a study in the External Dinarides, *Geophys J Int*, 205, 1694-1709, doi: 10.1093/gji/ggw106.

Kastelic, V., Vannoli, P., Burrato, P., Fracassi, U., Tiberti, M.M. & Valensise, G., 2013. Seismogenic sources in the Adriatic Domain, *Marine and Petroleum Geology,* 42, 191-213, doi: 10.1016/j.marpetgeo.2012.08.002.

Kastelic, V., Vrabec, M., Cunningham, D. & Gosar, A., 2008. Neo-Alpine structural evolution and present-day tectonic activity of the eastern Southern Alps: The case of the Ravne Fault, NW Slovenia, *Journal of Structural Geology,* 30, 963-975, doi: 10.1016/j.jsg.2008.03.009.

Kostrov, V.V., 1974. Seismic moment and energy of earthquakes and seismic flow of rock, *Izvestiya, Physics of the Solid Earth,* 1, 13-21.

Lavecchia, G., Boncio, P. & Creati, N., 2003. A lithospheric-scale seismogenic thrust in central Italy, *Journal of Geodynamics,* 36, 79-94, doi:10.1016/S0264-3707(03)00040-1.

Maesano, F.E., D'Ambrogi, C., Burrato, P. & Toscani, G., 2015. Slip-rates of blind thrusts in slow deforming areas: Examples from the Po Plain (Italy), *Tectonophysics,* 643, 8-25, doi: 10.1016/j.tecto.2014.12.007.

Maesano, F.E., Toscani, G., Burrato, P., Mirabella, F., D'Ambrogi, C. & Basili, R., 2013. Deriving thrust fault slip rates from geological modeling: Examples from the Marche coastal and offshore contraction belt, Northern Apennines, Italy, *Marine and Petroleum Geology,* 42, 122-134, doi: 10.1016/j.marpetgeo.2012.10.008.

Matrullo, E., De Matteis, R., Satriano, C., Amoroso, O., & Zollo A., 2013. An improved 1-D seismic velocity model for seismological studies in the Campania–Lucania region (Southern Italy), *Geophys. J. Int.*, **195**, 460–473, doi: 10.1093/gji/ggt224.

McCaffrey, R., 1997. Statistical significance of the seismic coupling coefficient, *Bull. Seism. Soc. Am.,* **87**, 1,069-1,073.

Montone, P. & Mariucci, M.T., 2016. The new release of the Italian contemporary stress map, doi: 10.1093/gji/ggw100.

Mucciarelli, M., Donda, F. & Valensise, G., 2015. Earthquakes and depleted gas reservoirs: which comes first? *Nat. Hazards Earth Syst. Sci.*, **15**, 2,201–2,208, doi:10.5194/nhess-15-2201-2015.

Rovida, A., Locati M., Camassi R., Lolli B., & Gasperini P. (eds), 2016. CPTI15, the 2015 version of the Parametric Catalogue of Italian Earthquakes. Istituto Nazionale di Geofisica e Vulcanologia. doi:http://doi.org/10.6092/INGV.IT-CPTI15.

Schorlemmer, D., S. Wiemer, and M. Wyss, 2005. Variations in earthquake-size distribution across different stress regimes, *Nature*, 437(7058), 539–542, doi:10.1038/nature04094.

Schorlemmer, D., Gerstenberger, M. C., Wiemer, S., Jackson, D. D, & Rhoades, D. A., 2007. Earthquake likelihood model testing, *Seismol. Res. Lett.*, 78(1), 17-29.

Schorlemmer, D., J. D. Zechar, J. D., Werner, M. J., Field, E. H., Jackson, D. D., Jordan, T. H. & the RELM Working Group, 2010. First results of the Regional Earthquake Likelihood Models experiment, *Pure Appl. Geoph.*, 167, 859-876.

Schorlemmer, D., Christophersen, A., Rovida, A., Mele, F., Stucchi, M. & Marzocchi, W., 2010. Setting up an earthquake forecast experiment in Italy, *Annals of Geophysics,* 53, 1-9, doi: 10.4401/ag-4844.

Stirling, M. W., McVerry, G.H., Gerstenberger, M.C., Litchfield, N.J., Van Dissen, R.J., Berryman, K.R., Barnes, P., Wallace, L.M., Villamor, P., Langridge, R.M., Lamarche, G., Nodder, S., Reyners, M.E., Bradley, B., Rhoades, D.A., Smith, W.D., Nicol, A., Pettinga, J., Clark, K.J., & Jacobs, K., 2012. National seismic hazard model for New Zealand : 2010 update, *Bull. Seism. Soc. Am.*, 102(4), 1,514-1,542; doi: 10.1785/0120110170.

Stucchi, M., Albini, P., Mirto, C., & Rebez, A., 2004. Assessing the completeness of Italian historical earthquake data, *Ann. Geophys.*, 47 (2/3), 659-673, doi: 10.4401/ag-3330.

Stucchi, M., Meletti, C., Montaldo, V., Crowley, H., Calvi, G. M., & Boschi, E., 2011. Seismic hazard assessment (2003–2009) for the Italian Building Code, *Bull. Seism. Soc. Am.*, 101 (4), 1,885-1,911, doi: 10.1785/0120100130.

Tarabusi, G., & Caputo, R., 2016. The use of HVSR measurements for investigating buried tectonic structures: the Mirandola anticline, Northern Italy, as a case study, *R. Int. J. Earth. Sci. (Geol. Rundsch.)*, **105**, 1-13, doi:10.1007/s00531-016-1322-3

Tiberti, M. M., Vannoli, P., Fracassi, U., Burrato, P., Kastelic, V., & Valensise, G., 2016. Understanding seismogenic processes in the Southern Calabrian Arc: a geodynamic perspective, *Italian Journal of Geoscience*, in press.

Tiberti, M.M., Orlando, L., Di Bucci, D., Bernabini, M. & Parotto, M., 2005. Regional gravity anomaly map and crustal model of the Central-Southern Apennines (Italy), *Journal of Geodynamics*, 40, 73-91, doi: 10.1016/j.jog.2005.07.014.

Valensise, G., & Pantosti, D. (eds.), 2001b. Database of Potential Sources for Earthquakes Larger than M 5.5 in Italy, *Annali di Geofisica*, 44 (4), Suppl. 1, 183 pp. (with CD-ROM).

Valensise, G., & Pantosti, D. 2001a. The investigation of potential earthquake sources in peninsular Italy: a review, *J. Seismol.*, 5, 287-306, doi: 10.1023/A:1011463223440.

Vannoli, P., Basili, R. & Valensise, G., 2004. New geomorphic evidence for anticlinal growth driven by blind-thrust faulting along the northern Marche coastal belt (central Italy), *Journal of Seismology*, 8, 297-312, doi: 10.1023/B:JOSE.0000038456.00574.e3.

Vannoli, P., Burrato, P., & Valensise, G., 2015. The seismotectonics of the Po Plain (Northern Italy): tectonic diversity in a blind faulting domain, *Pure And Applied Geophysics*, 172, 1,105-1,142, doi: 10.1007/s00024-014-0873-0.

Ward, S.N., 1994. A Multidisciplinary Approach to Seismic Hazard in Southern California, *Bull. Seism. Soc. Am.*, 84, 1293-1309.

Woessner, J. & Wiemer, S., 2005. Assessing the Quality of Earthquake Catalogues: Estimating the Magnitude of Completeness and Its Uncertainty, doi: 10.1785/0120040007.

Woessner, J., Danciu, L., Giardini, D., Crowley, H., Cotton, F., Grünthal, G., Valensise, G., Arvidsson, R., Basili, R., Demircioglu, M. B., Hiemer, S., Meletti, C., Musson, R. W., Rovida, A. N., Sesetyan, K., & Stucchi, M., 2015. The 2013 European Seismic Hazard Model: key components and results, *Bulletin of Earthquake Engineering*, 13, 3553-3596, doi: 10.1007/s10518-015-9795-1.

Zechar, J. D., Gerstenberger, M. C. & Rhoades, D. A., 2010. Likelihood-based tests for evaluating space-rate-magnitude earthquakes, *Bull. Seismol. Soc. Am.*, 100(3), 1184-1195.

Tables

Table 1. Seismicity parameters, coupled thicknesses, and coupling by faulting class. A question mark next to a parameter indicates that we could not determine the upper limit for that parameter.

	Subcatalogues based on fault kinematics		
	CF Compressional faults	EF Extensional Faults	SS Strike-slip Faults
C_{class}/L_{class}, earthquakes/km	0.0379	0.0867	0.0270
Earthquakes from CPTI15 1880-2013, m_t=4.8	147.7	154.3	44.1
Asymptotic slope β	$0.71^{+0.14}_{-0.12}$	$0.63^{+0.14}_{-0.11}$	$0.71^{+0.14}_{-0.12}$
Corner magnitude m_c	$6.62^{+?}_{-0.3}$	$7.17^{+?}_{-0.35}$	$6.62^{+?}_{-0.3}$
Seismic moment rate $\dot{M}_{seis}$, N m/s×10^9	$128^{+?}_{-33}$	$32.3^{+?}_{-11.5}$	$3.8^{+?}_{-1.0}$
Shear modulus μ, GPa	$35.2^{+5.4}_{-6.0}$	$35.2^{+5.4}_{-6.0}$	$35.2^{+5.4}_{-6.0}$
Average fault-to-$\hat{\dot{\varepsilon}}_{great}$ angles, $\theta_1 = \theta_2$, °	35	49	76
Coupled thickness , km	$3.7^{+?}_{-1.4}$	$7.2^{+?}_{-3.3}$	$4.8^{+?}_{-1.9}$
Coupled thickness considering only μ and kinematic model uncertainties, km	$3.7^{+0.7}_{-0.7}$	$7.2^{+2.5}_{-1.5}$	$4.8^{+0.9}_{-0.9}$

Table 2. Diffusivity determined for each faulting class over the six best models reported in Carafa & Bird (2016) using the average dip reported in Table 1.

Model	$A_0(\cdot 10^8)$ **m²**	**Diffusivity CF (·10³ m²/yr)**	**Diffusivity EF (·10³ m²/yr)**	**Diffusivity SS (·10³ m²/yr)**
1	12	27.7	32.8	6.4
2	14	28.5	36.5	6.7
3	16	29.5	39.9	6.4
4	18	30.0	42.7	7.1
5	20	31.7	45.5	7.3
6	22	32.7	47.7	7.7

Figures

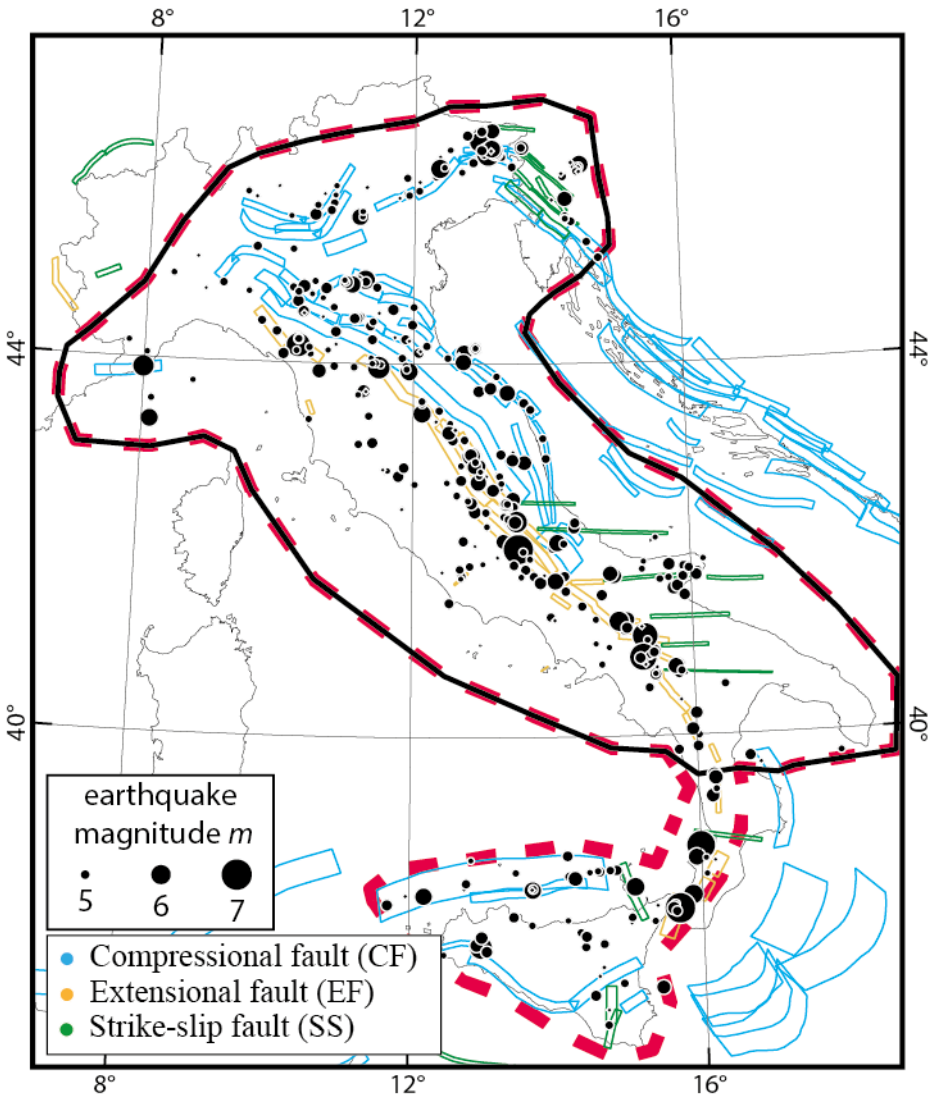

Figure 1. Black circles: CPTI15 catalogue (1880-2013, m_t=4.8); blue, yellow and green polylines: surface trace of DISS Composite Seismogenic Sources (DISS Working Group 2015). Seismicity is forecast for the region enclosed by the black polyline, whereas earthquakes inside the region enclosed by the dashed red polyline are used for determining the magnitude-frequency distribution parameters.

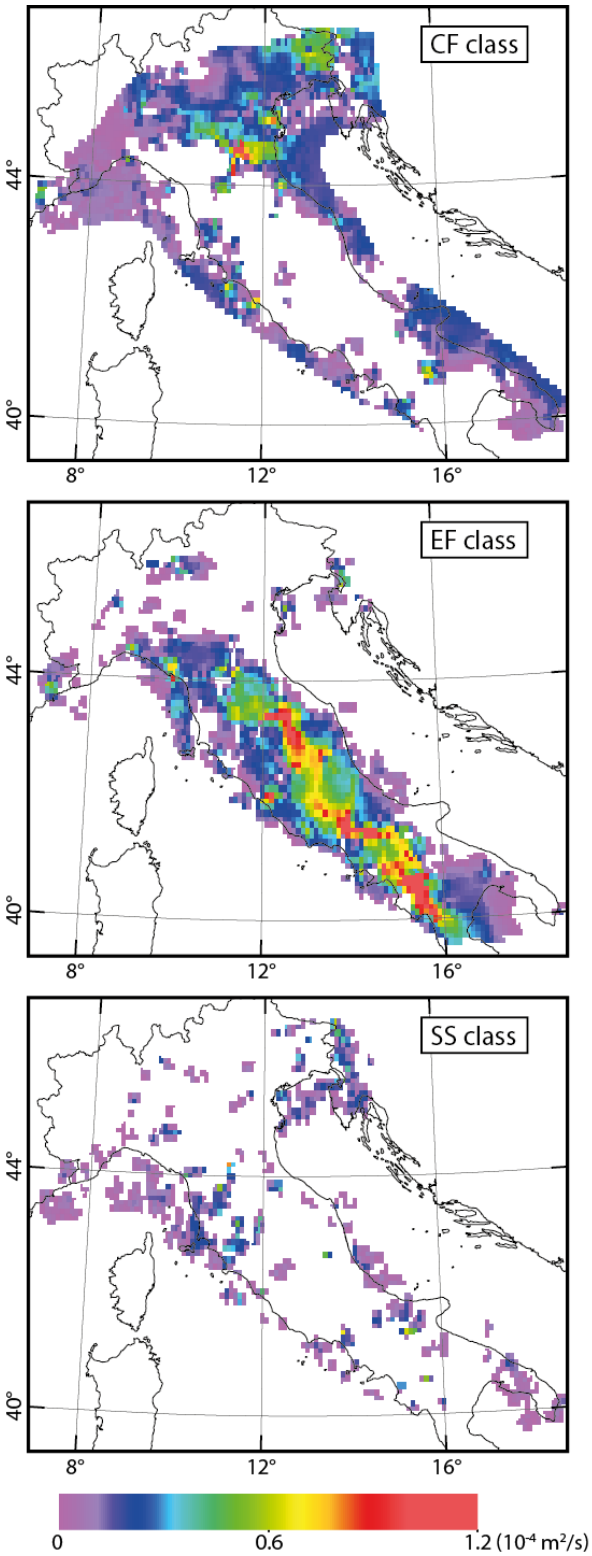

Figure 2. Long-term diffusivity for the CF (top), EF (center), and SS (bottom) faulting classes, determined for one of the six best models (Experiment3, model A_0=18·10^8 m^2) reported in Carafa & Bird (2016).

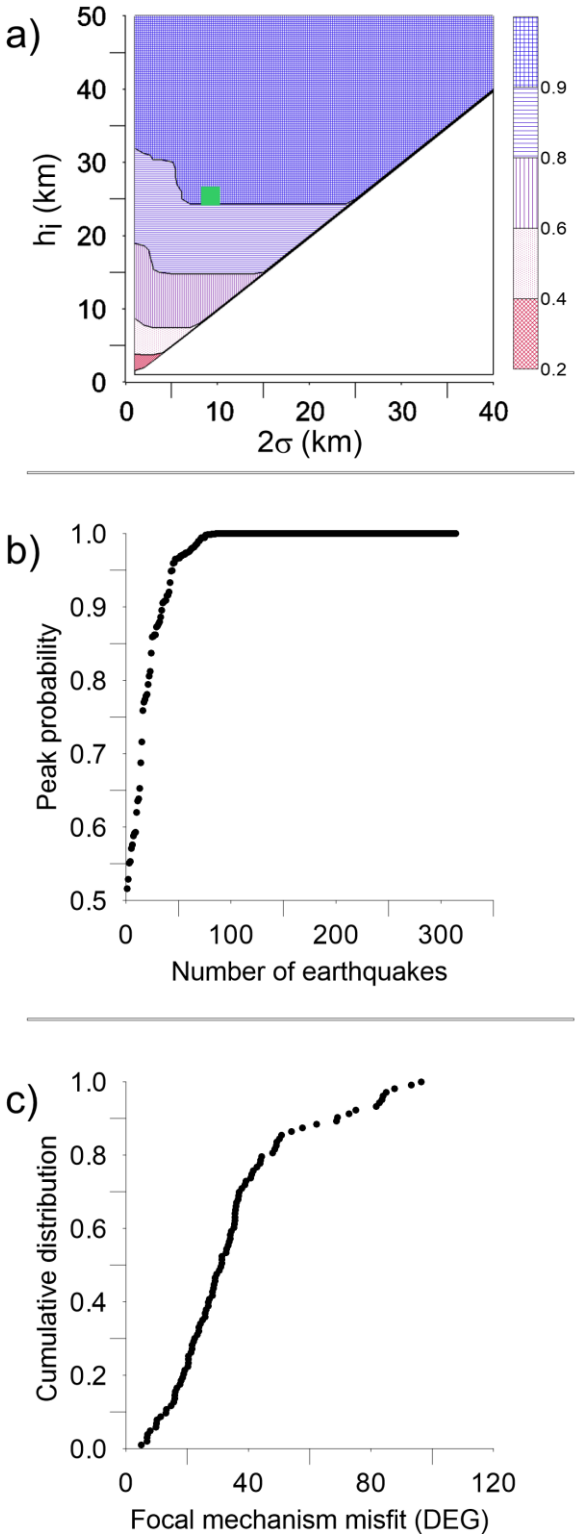

Figure 3. a): fraction of the earthquake sample from CPTI15 assigned to DISS faults. The green square indicates the $h_i - 2\sigma$ values selected for DISS database. b) Cumulative distribution of peak probabilities for the 314 earthquakes assigned to faults. c): Cumulative distribution of misfit between DISS-predicted and observed focal mechanisms reported in Montone & Mariucci (2016).

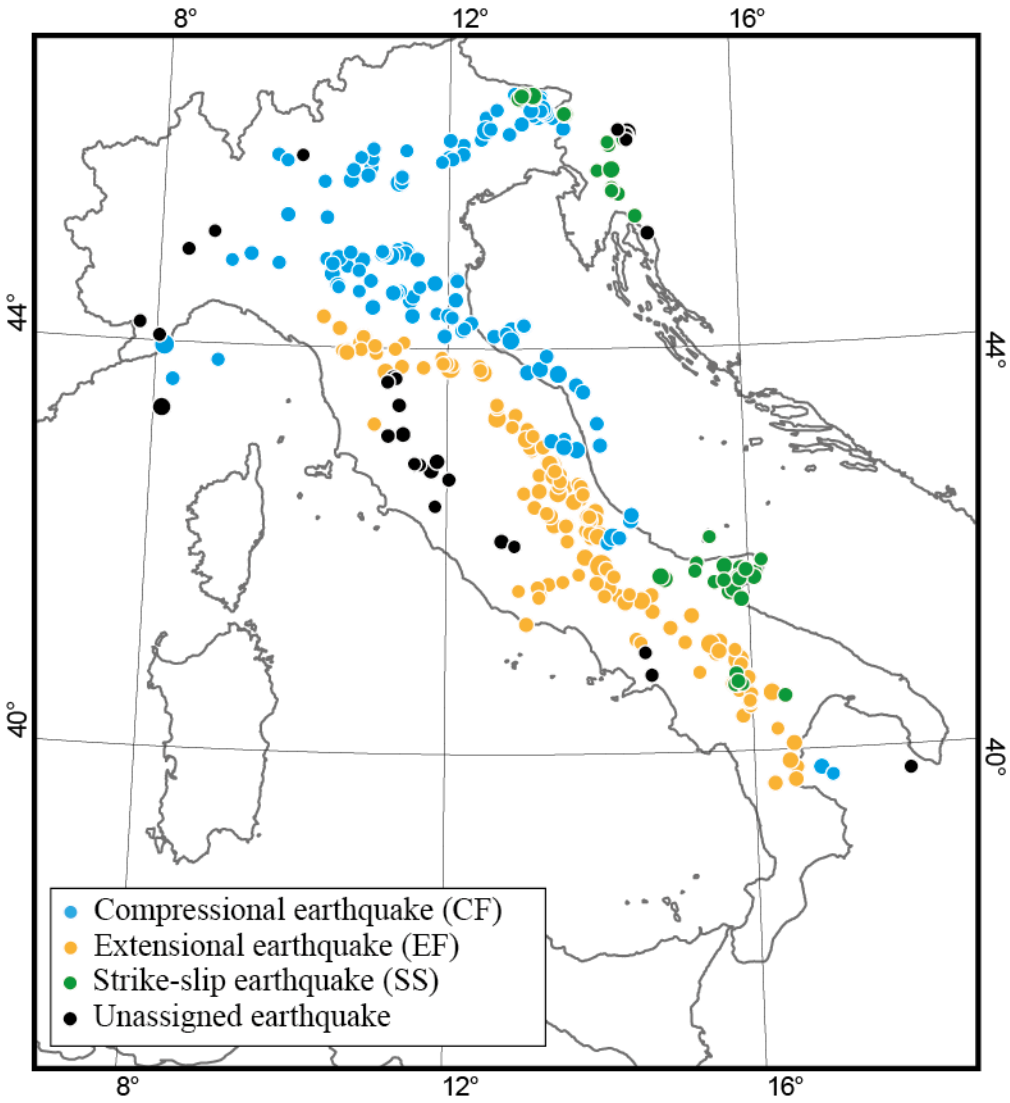

Figure 4. CPTI15 earthquakes (1880-2013, m_t=4.8), color-coded to the relevant faulting class.

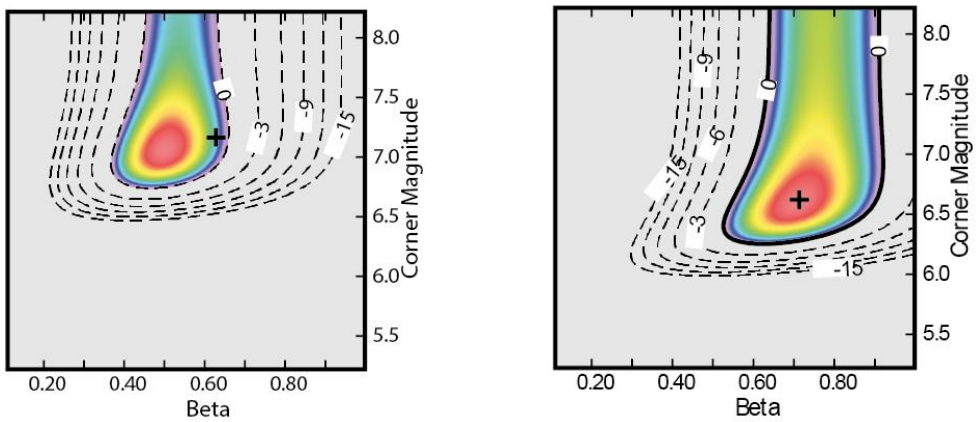

Figure 5. Contour maps of relative log-likelihood illustrating the fit of a tapered Gutenberg-Richter frequency/moment distributions to the CPTI15 catalogue (1787-2013, m_t=5.22). The cross indicates the most likely β - M_c pair along the column with best estimate of β obtained from the more complete truncated CPTI15 catalogue (1880-2013, m_t=4.8). Left: β - M_c grid for the EF class. Right: β - M_c grid for the CF and SS classes.

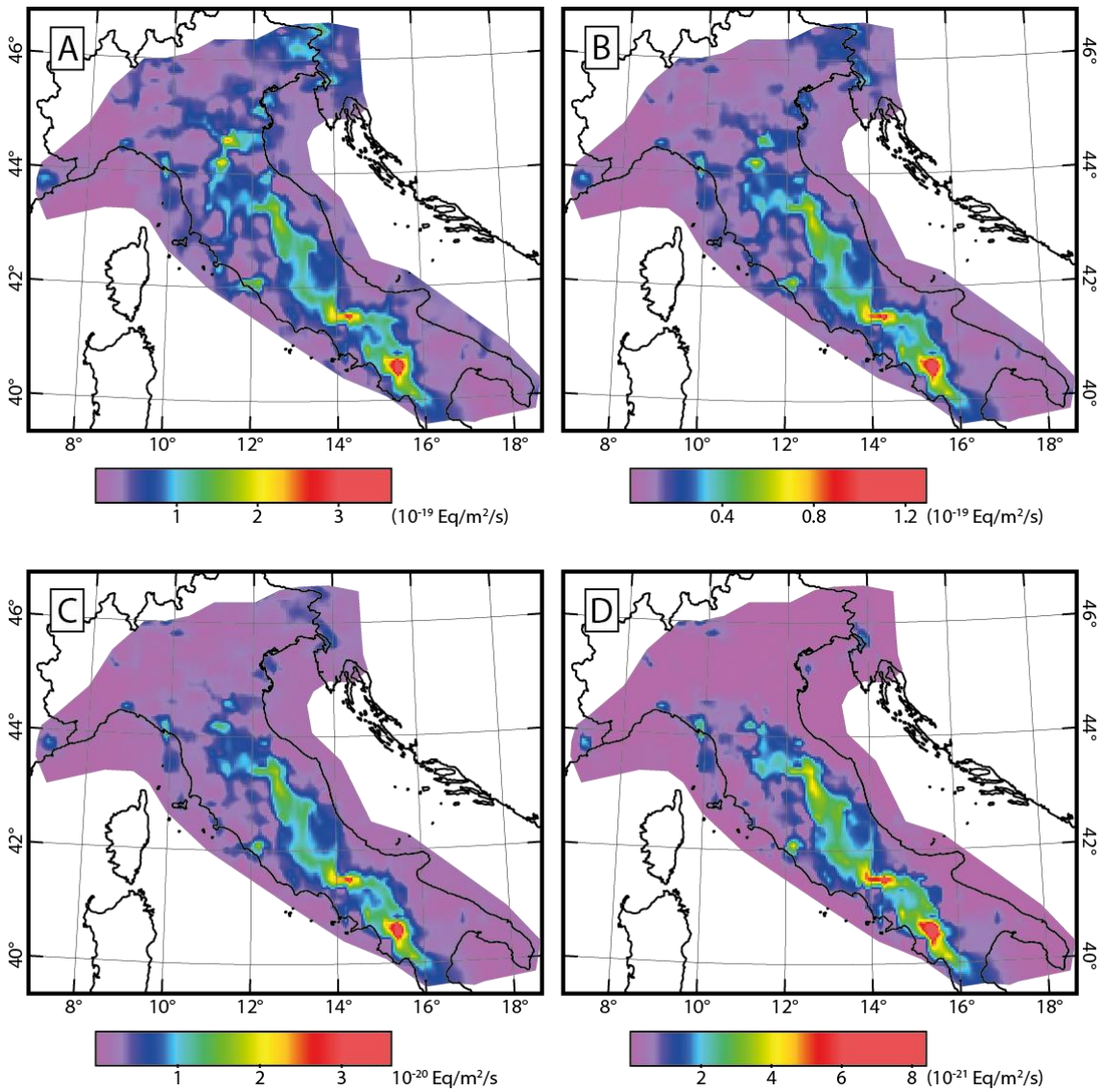

Figure 6. Forecast long-term seismicity (earthquake epicenters per square meter per second, including aftershocks) in the study region. From top to bottom, left to right: m_t=5.5, m_t=6.0, m_t=6.5, m_t=7.0.

Appendix 1. Tectonic moment rate using horizontal-plane strain-rate tensors

Let us consider the three principal values of the long-term strain-rate tensors $\dot{\varepsilon}_1 \le \dot{\varepsilon}_2 \le \dot{\varepsilon}_3$. As in Section 2, here we re-label them as

$$\dot{\varepsilon}_{\text{great}} = \sup(|\dot{\varepsilon}_1|, |\dot{\varepsilon}_2|, |\dot{\varepsilon}_3|) \quad \text{(A1)}$$

$$\dot{\varepsilon}_{\text{least}} = \inf(|\dot{\varepsilon}_1|, |\dot{\varepsilon}_2|, |\dot{\varepsilon}_3|) \quad \text{(A2)}$$

$$\dot{\varepsilon}_{\text{mid}} = \dot{\varepsilon}_{\text{great}} - \dot{\varepsilon}_{\text{least}} \quad \text{(A3)}$$

In this appendix we show that the tectonic moment rate $\dot{M}_{tect}$ of a lithosphere volume is dependent not only on strain-rate and shear modulus but also on the orientations of active faults of the investigated lithosphere. Accordingly, we propose an appropriate formulation to determine a kinematically-consistent $\dot{M}_{tect}$. In detail, the formulation of *Ward* [1994] to calculate $\dot{M}_{tect}$ is:

$$\dot{M}_{\text{tect}} = 2 \cdot \mu \cdot A \cdot z \cdot \dot{\varepsilon}_{\text{great}} \quad \text{(A4)}$$

while here we suggest a more general formulation

$$\dot{M}_{\text{tect}} = k \cdot \mu \cdot A \cdot z \cdot \dot{\varepsilon}_{\text{great}} \quad \text{(A5)}$$

and that a different k factor (not the $k = 2$ of *Ward* [1994]) needs to be considered if the active-fault planes in the modeled volume of lithosphere are not at angles of $\theta = 45°$ from $\hat{\dot{\varepsilon}}_{\text{great}}$, the greatest (in magnitude) strain-rate principal axis.

Let us assume a coordinate system with *x*-axis parallel to $\hat{\dot{\varepsilon}}_{\text{great}}$, *y*-axis parallel to $\hat{\dot{\varepsilon}}_{\text{mid}}$ and *z*-axis parallel to $\hat{\dot{\varepsilon}}_{\text{least}}$ and let us investigate the moment rate of the more active conjugate fault as shown in Figure A1. Note that the drawing does not display a cubic volume; instead, we choose a rectangular solid element with relative dimensions $dy = dx \tan\theta_1$ and $dz = dx \tan\theta_2$ with θ_1 being the angle between $\hat{\dot{\varepsilon}}_{\text{great}}$ and the more-active fault system and θ_2 between $\hat{\dot{\varepsilon}}_{\text{great}}$ and the less-active fault system. In Figure A1 all 4 faults intersect the corners of the volume, and inward-or-outward displacements of each face of the volume element are uniform across each facet.

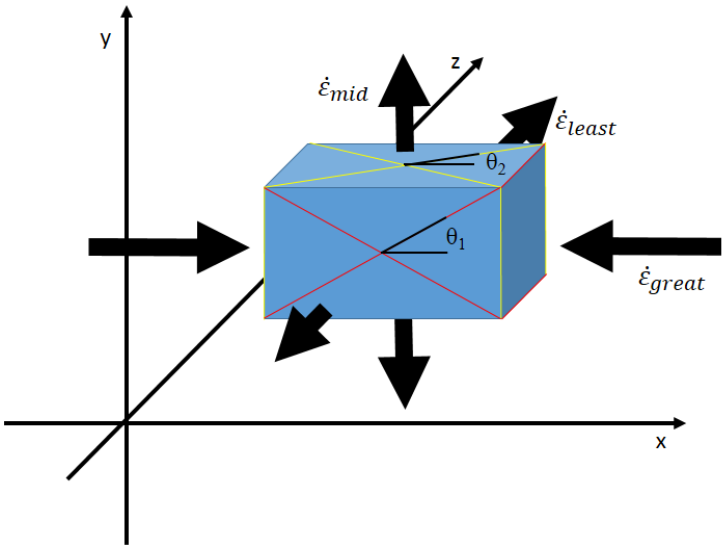

Figure A1. Deforming rectangular solid element.

The length dl of the less-active faults outcropping on the front face of the cube is dz, while the width dw can be expressed as $dx/\cos\theta_1$ and the sum of the two conjugate slip-rates, $d\dot{s}$, can be expressed as $\dot{\varepsilon}_{\text{mid}} \cdot dy/\sin\theta_1$. The moment rate $\dot{M}_{f1}$ of such a fault system is

$$\dot{M}_{f1} = \mu \cdot dl \cdot dw \cdot d\dot{s} = \mu \cdot dx \cdot dy \cdot dz \cdot \dot{\varepsilon}_{\text{mid}} \cdot \frac{1}{\cos(\theta_1)\sin(\theta_1)} \qquad \text{(A6)}$$

For the more-active faults outcropping on the top face of the cube, the width dw can be expressed as dy ; dl is equal to $dx/\cos\theta_2$ and the sum of the two conjugate slip-rates is $\dot{\varepsilon}_{\text{least}} \cdot dz/\sin\theta_2$ resulting in an infinitesimal moment rate $\dot{M}_{f2}$

$$\dot{M}_{f2} = \mu \cdot dl \cdot dw \cdot d\dot{s} = G \cdot dx \cdot dy \cdot dz \cdot \dot{\varepsilon}_{\text{least}} \cdot \frac{1}{\cos(\theta_2)\sin(\theta_2)} \qquad \text{(A7)}$$

The total moment rate of the volume is then

$$\dot{M}_{\text{vol}} = \dot{M}_{f1} + \dot{M}_{f2} = \mu \cdot dx \cdot dy \cdot dz \cdot \left(\frac{\dot{\varepsilon}_{\text{med}}}{\cos(\theta_1)\sin(\theta_1)} + \frac{\dot{\varepsilon}_{\text{least}}}{\cos(\theta_2)\sin(\theta_2)} \right) \qquad \text{(A8)}$$

whereas in the volume $\Delta V = A \cdot z$ of a lithosphere with homogeneous strain rates and fault angles the tectonic moment rate is

$$\dot{M}_{\text{tect}} = \mu \cdot A \cdot z \cdot \left(\frac{\dot{\varepsilon}_{\text{med}}}{\cos(\theta_1)\sin(\theta_1)} + \frac{\dot{\varepsilon}_{\text{least}}}{\cos(\theta_2)\sin(\theta_2)} \right) \qquad \text{(A9)}$$

with

$$\left(\frac{\dot{\varepsilon}_{\text{med}}}{\cos(\theta_1)\sin(\theta_1)} + \frac{\dot{\varepsilon}_{\text{least}}}{\cos(\theta_2)\sin(\theta_2)} \right) = k \cdot \dot{\varepsilon}_{great} \qquad \text{(A10)}$$

In the particular case of $\theta_1 = \theta_2 = 45°$,

$$\left(\frac{\dot{\varepsilon}_{\text{med}}}{\cos(\theta_1)\sin(\theta_1)} + \frac{\dot{\varepsilon}_{\text{least}}}{\cos(\theta_2)\sin(\theta_2)} \right) = 2 \cdot \left(\dot{\varepsilon}_{\text{med}} + \dot{\varepsilon}_{\text{least}} \right) = 2 \cdot \dot{\varepsilon}_{\text{great}} \qquad \text{(A11)}$$

as suggested by *Ward* [1994]. This is a realistic factor only if $\theta_1 = \theta_2 \simeq 45°$ and different values of θ_1 and θ_2 are expected to result in different $\dot{M}_{tect}$ estimates. For example, let us assume that the principal strain rate axes are parallel to the principal stress axes and recall the Coulomb-Navier criterion, which empirically shows that

$$\tan 2\theta_1 = \frac{1}{f} \qquad \text{(A12)}$$

where f is the average fault friction of a determined fault system. Setting $k = 2$ implies $\theta_1 = \theta_2 = 45°$ which then implies two frictionless fault sets. If we alternatively consider $f = 0.6$ in Equation (A12), we obtain $\theta_1 = \theta_2 = 60°$ (for extensional $\dot{\varepsilon}_{great}$) or $\theta_1 = \theta_2 = 30^{\circ}$ (for compressional $\dot{\varepsilon}_{\text{great}}$) and $k = \left(\frac{\dot{\varepsilon}_{\text{med}}}{\cos(\theta_1)\sin(\theta_1)} + \frac{\dot{\varepsilon}_{\text{small}}}{\cos(\theta_2)\sin(\theta_2)} \right) = 2.31 \cdot \dot{\varepsilon}_{\text{great}}$ with a net increase of moment rate estimation of 15% just due to a different friction value assigned to active fault sets.